

Abundance patterns of multiple populations in Globular Clusters: a chemical evolution model based on yields from AGB ejecta

Annibale D’Ercole,^{1*} Francesca D’Antona,² Paolo Ventura,²
 Enrico Vesperini³ and Stephen L. W. McMillan³

¹*INAF- Osservatorio Astronomico di Bologna, via Ranzani 1, I-40127 BOLOGNA (Italy)*

²*INAF- Osservatorio Astronomico di Roma, via di Frascati 33, I-00040 Monteporzio (Italy)*

³*Department of Physics, Drexel University, Philadelphia, PA 19104, USA*

Accepted ... Received ...; in original form ...

ABSTRACT

A large number of spectroscopic studies have provided evidence of the presence of multiple populations in globular clusters by revealing patterns in the stellar chemical abundances. This paper is aimed at studying the origin of these abundance patterns. We explore a model in which second generation (SG) stars form out of a mix of pristine gas and ejecta of the first generation of asymptotic giant branch stars. We first study the constraints imposed by the spectroscopic data of SG stars in globular clusters on the chemical properties of the asymptotic and super asymptotic giant branch ejecta. With a simple one-zone chemical model, we then explore the formation of the SG population abundance patterns focussing our attention on the Na-O, Al-Mg anticorrelations and on the helium distribution function.

We carry out a survey of models and explore the dependence of the final SG chemical properties on the key parameters affecting the gas dynamics and the SG formation process. Finally, we use our chemical evolution framework to build specific models for NGC 2808 and M4, two Galactic globular clusters which show different patterns in the Na-O and Mg-Al anticorrelation and have different helium distributions. We find that the amount of pristine gas involved in the formation of SG stars is a key parameter to fit the observed O-Na and Mg-Al patterns. The helium distribution function for these models is in general good agreement with the observed one. Our models, by shedding light on the role of different parameters and their interplay in determining the final SG chemical properties, illustrate the basic ingredients, constraints and problems encountered in this self-enrichment scenario which must be addressed by more sophisticated chemical and hydrodynamic simulations.

Key words: stars: chemically peculiar – globular clusters: general – globular clusters: NGC 2808, NGC 6121 (M4)

1 INTRODUCTION

In the last decade, a large number of spectroscopic and photometric studies have provided strong indication of the presence of multiple stellar populations in globular clusters.

The spectroscopic evidence comes from the observed spreads and anticorrelations between the abundances of light elements, not shown by the halo stars of similar metallicities. Specifically, all the clusters studied have shown an anticorrelation between Na and O and an anticorrelation be-

tween Mg and Al has been found in several massive clusters (cf. Gratton et al. 2004). The fact that these chemical anomalies have been found also in turnoff and subgiant stars (Gratton et al. 2001; Ramírez & Cohen 2002) indicates that they must be already present in the gas from which these stars formed. The anticorrelation between CN and CH bands observed in giant (e.g. Norris et al. 1984) and turnoff stars indicates a difference in the nitrogen abundance and is considered another fingerprint of the presence of multiple populations in globular clusters.

An additional important constraint on the possible sources of gas from which second generation stars formed

* E-mail: annibale.dercole@oabo.inaf.it

is provided by the observed constancy of the total C+N+O. The only exception, so far, is NGC 1851 for which a difference of 0.6 dex is found among four red giants (Yong et al. 2009) and for which the analysis of the subgiant branch suggests that the total C+N+O increases by about a factor three between the stars in the brighter and those in the dimmer branch (Ventura et al. 2009).

Photometric studies have also provided a number of important results indicating the presence of significant differences in the helium abundances of stars within individual clusters. Indeed, the presence of helium differences seems to be the only explanation for the multiple main sequences or spread in the main sequence (MS) observed in some clusters. These observations confirmed the prediction of the presence of a helium spread based on the complex morphology of the horizontal branches of some clusters made by (D’Antona & Caloi 2004, 2008). In extreme cases (the blue MS of ω Cen and of NGC 2808) a helium content $Y=0.38-0.40$ is inferred (Norris 2004; D’Antona et al. 2005; Piotto et al. 2007).

A recent spectroscopic survey by Carretta et al. (2009c) has found that all the 15 clusters studied show the spectroscopic evidence of the presence of multiple populations and that in all cases second generation stars represent a significant fraction (50-80 %) of a cluster population. This implies that matter forming more than half of each cluster stars has been processed through the hot CNO cycle and by other proton-capture reactions on light nuclei.

In spite of the light elements variation, most GCs are mono-metallic objects, as far as abundances of heavier elements are concerned (see Gratton et al. 2004, for a recent review on this subject). Their heavy ($Z > 13$) element metallicity, usually represented by the ratio $[\text{Fe}/\text{H}]$, is found to be extremely homogeneous from star to star in each cluster. Carretta et al. (2009a) find that the upper limit to the scatter of iron is less than 0.05 dex in the 19 clusters they examine. This is consistent with previous determinations, e.g. for NGC 6752 ($\sigma=0.02$ Yong et al. 2005), and for the clusters examined by Kraft & Ivans (2003) (0.03 – 0.10 dex). The width in color of the main sequence and/or of the red giant branch also agree with the spectroscopic determination (Suntzeff 1993). As the site of production of heavy elements (α -capture and Fe-group elements) are stars exploding as core-collapse or thermonuclear supernovae (e.g. Wheeler et al. 1989), the star to star iron homogeneity means that supernova ejecta do not affect the chemistry of the gas processed through the hot CNO cycle. On the other hand, significant iron and s-process elements spread is well known to be present in ω Cen (e.g., for a recent analysis, Johnson et al. 2009, and references therein) and more recently it has been confirmed in other massive clusters like M22 (Marino et al. 2009; Da Costa et al. 2009, and references therein), M54 (Sarajedini & Layden 1995; Bellazzini et al. 2008, and references therein), and Terzan 5 (Ferraro et al. 2009). In smaller clusters like NGC 1851, the SG might be enriched in calcium, according to Lee et al. (2009), but see the discussion by Carretta et al. (2010).

In D’Ercole et al. (2008) (hereafter Paper I), we presented a model for the formation and dynamical evolution of multiple populations in globular clusters (GCs). In particular, we explored a model in which second generation (hereafter SG) stars form out of the ejecta of the first generation

(hereafter FG) stars. By means of hydrodynamic simulations we have shown that the ejecta of AGB (asymptotic giant branch) stars collect in a cooling flow into the cluster core, where they form a subsystem of SG stars initially strongly concentrated in the cluster innermost regions. By means of N-body simulations we have then explored the subsequent stellar dynamical evolution of the cluster focusing our attention on the early loss of FG stars, on the evolution of the ratio of the number of FG and SG stars and on the evolution of their relative spatial distribution and mixing.

Paper I also included a preliminary discussion on the chemical abundances of FG AGB stars and on the possibility of reproducing the helium excess and other chemical anomalies observed in SG stars. Several theoretical and observational papers have shown that dilution of the FG ejecta with gas having the pristine composition is needed to explain the general shape of the anticorrelations (Prantzos et al. 2007; Bekki et al. 2007; D’Antona & Ventura 2007; Carretta et al. 2009c). If the SG anomalies are imputed to processing by Hot Bottom Burning (HBB) at the bottom of the convective envelope of massive AGBs, these models produce a direct correlation between sodium and oxygen abundance in the processed matter. This direct correlation is unavoidable, as found in all the relevant AGB computations (Denissenkov & Herwig 2003; Herwig 2004; Karakas & Lattanzio 2007; Ventura & D’Antona 2008b) and as explained in more detail in Section 2. While the total sodium yield is dependent on many uncertain factors, it is certain that a small oxygen depletion (lower burning temperature) goes together with a larger sodium abundance and a large oxygen depletion (higher burning temperature) is accompanied by a smaller sodium abundance. Any attempt to reverse this direct correlation, in the limits provided by available cross sections, has been unfruitful (e.g. Ventura & D’Antona 2008b). An observational hint in favour of the above arguments is given by Carretta et al. (2009c) who find a direct correlation between the minimum O and the maximum Na abundances of the 15 clusters they studied; such a result could not be understood if O and Na of the AGB ejecta were anticorrelated.

From all the above, it is apparent that, in order to explain the GC chemical patterns, it is necessary to introduce a form of dilution of the AGB ejecta, either with pristine gas, or with gas not showing the peculiar abundance patterns of the hot-CNO processed matter.

The source of this pristine matter still requires a detailed understanding. D’Ercole et al. (2008) proposed that initial asymmetries in the gas distribution allow to vent out the Type II supernovae (SNe II) ejecta along preferential directions, creating an “hour-glass” cavity and leaving some pristine gas in a torus at the outskirts of the cluster; at the end of the SN II activity this torus eventually collapses back into the cluster. In this scenario, the torus is not affected by contamination from supernova ejecta, and the iron content of the diluting matter is still the pristine one, consistently with the absence of iron differences between the FG and SG summarized above. While the evolution of the larger clusters is probably also affected by more prolonged star formation and supernovae type Ia contamination (e.g. Marcolini et al. 2007), the presence of slight metal increase in smaller clusters might be a possible indication that the “pristine” gas

in the falling back torus has been partially contaminated by the SN II ejecta.

This paper is aimed at significantly expanding the initial study of SG stars chemical abundances presented in Paper I and at exploring in detail the SG chemical anomalies emerging from a model in which SG stars form from a mix of AGB ejecta and gas with pristine chemical composition.

We will refer to the scenario presented in Paper I. Consequently, we need to associate to the temporal evolution of the FG clusters the chemical composition of the ejecta of super-AGB and then massive AGB stars (hereinafter simply referred to as AGB polluters) that successively provide the matter used for building up second generation stars. The chemical composition of the H-rich matter in the envelopes of these stars is affected by the hot CNO cycle processing at the basis of the convective envelope of these giants (hot bottom burning, hereafter HBB) and possibly also by the third dredge up (3DU) occurring after each thermal pulse. Stellar winds and planetary nebula ejection deposit the matter of these envelopes into the interstellar medium (ISM), where it can contribute to the formation of the second generation.

Despite the significant effort devoted to the determination of the yields of the massive AGBs and the numerous attempts to quantify the uncertainties in these calculations (Ventura & D’Antona 2005a,b; Karakas & Lattanzio 2007), there are still large differences in the results obtained by different groups and even by the same groups at different times and no general consensus has been reached.

Our aim is to focus on the chemical properties of the stellar envelopes and explore the constraints on these properties imposed by the spectroscopic data of SG stars in globular clusters. We have addressed this problem by means of a simple one-zone model in which the ISM is supplied by the FG AGB ejecta and by the possible accretion of pristine gas, and is depleted by the SG star formation (hereafter SF). This simplified approach allows to easily control the evolution of the amount of the AGB ejecta and pristine gas involved in the SG formation process and to fully explore the chemical properties of the ISM and of the SG stars.

The structure of the paper is the following. We start in sect. 2 with an overview of the chemical abundances of the massive AGB ejecta. We then illustrate our general assumptions in sect. 3 and the model details in sect. 4. We then analyze the model in sect. 5, and compare our results with the data of NGC 2808 and M4 in sect. 6.1 and sect. 6.2, respectively. Finally, we summarize our conclusions in sect. 7.

2 EDUCATED GUESSES ON THE YIELDS FROM SUPER-AGB AND MASSIVE AGB STARS

We start by re-examining all the uncertainties connected with the computation of the chemical yields of the AGB polluters, identifying the range of possible models producing chemical patterns and trends consistent with those found in spectroscopic observational studies. We will adopt yields for massive AGBs listed in Table 2 in Ventura & D’Antona (2009) for metallicity $Z=10^{-3}$ (see Fig. 1), and in Table 1, modified and extrapolated as shown in the columns labelled “n”. For carbon and nitrogen, the abundances of

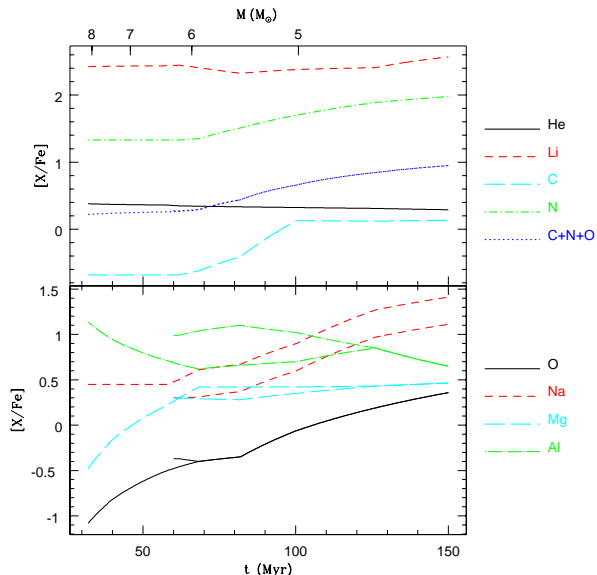


Figure 1. Time evolution of the chemical abundance of the ejecta of the dying stars adopted in this paper (thick lines) and as given by Ventura & D’Antona (2009) (thin lines). On the top axis some masses of dying stars are reported in correspondence to their lifetime.

Ventura & D’Antona (2009) are adopted without modification (for 6.5 and 9 M_{\odot} , the values of $M=6.3 M_{\odot}$ have been adopted).

We list in the next subsections the problems relative to each individual chemical element, and how they are related to the physical inputs (e.g. cross sections) or to the treatment of some important structural problems (e.g. the treatment of convection, mass loss, possible extra-mixing at the formal convective boundaries). We will mainly deal with the yields relative to the metallicity $Z=10^{-3}$, $[\alpha/Fe]=0.4$, for two reasons: 1) this metallicity is adequate to describe most of the GCs for which data relevant for the study of the chemical anomalies are available; 2) this is the metallicity for which most theoretical models have been built (see Ventura & D’Antona 2008a,b, 2009, for yields calculated for different values of Z).

2.1 The role of super-AGBs and their yields

Most researchers focused on the problem of multiple stellar populations mainly when two clusters (ω Cen and NGC 2808) were recognized to have a large fraction of main sequence stars ($\sim 25\%$ in ω Cen, $\sim 15\%$ in NGC 2808) in a “blue MS” which could only be interpreted as a very helium rich MS (Bedin et al. 2004; Norris 2004; Piotto et al. 2005; D’Antona et al. 2005; Piotto et al. 2007)¹. In both clusters, this extreme-helium population must also be very *homogeneous*, both in helium and metal content, otherwise the blue MS would not be detached from the rest of MS stars. Two other very massive clusters, NGC 6441 and NGC 6388, show an horizontal branch (HB) extended to very high- T_{eff} ,

¹ Actually, Piotto et al. (2007) show that in NGC 2808 three different parts of the MS can be identified.

Table 1. Averaged abundances in the ejecta of massive AGB and super-AGB stars.

M/M_{\odot}	$\tau/10^6{}^a$	$M_c/M_{\odot}{}^b$	Y	[O/Fe] ^d	[O/Fe] _n ^e	[Na/Fe] ^d	[Na/Fe] _n ^e	[Mg/Fe] ^d	[Mg/Fe] _n ^e	[Al/Fe] ^d	[Al/Fe] _n ^e
3.0	332	0.76	0.248	0.92	0.92	1.16	1.46	0.57	0.57	0.65	0.65
3.5	229	0.80	0.265	0.77	0.77	1.30	1.60	0.55	0.55	0.66	0.66
4.0	169.5	0.83	0.281	0.44	0.44	1.18	1.48	0.48	0.48	0.55	0.55
4.5	130.3	0.86	0.310	0.19	0.19	0.97	1.27	0.43	0.43	0.85	0.85
5.0	103.8	0.89	0.324	-0.06	-0.06	0.60	0.90	0.35	0.42	1.02	0.70
5.5	85.1	0.94	0.334	-0.35	-0.35	0.37	0.67	0.28	0.42	1.10	0.66
6.0	71.2	1.00	0.343	-0.40	-0.40	0.31	0.61	0.29	0.42	1.04	0.62
6.5	61.5	1.05	0.360 ^c		-0.50		0.45		0.22		0.71
9.0	32.0	1.37	0.380 ^c		-1.10		0.45		-0.50		1.15

^aTotal evolutionary time until the AGB phase^bCore mass at the beginning of the AGB phase.^cFrom Siess (2007a).^dFrom Ventura & D’Antona (2009).^eValues adopted in this paper.

and their RR Lyr variables have very long periods, indicating very high RR Lyr luminosity, a peculiar occurrence at the high metallicity of these clusters (Rich et al. 1997). Also in these cases, a very high helium population (including $\sim 10\%$ and $\sim 20\%$ of stars respectively) provides the only reliable explanation for these features (Caloi & D’Antona 2007; Busso et al. 2007; Yoon et al. 2008),

In all cases, modelling the MS colours, or the HB morphology and the RR Lyr periods, the helium content of the most extreme population results to be $Y \sim 0.38\text{--}0.42$. Values so high are extremely peculiar, particularly because the helium enrichment *is not* accompanied by metal enrichment (a value ~ 70 is estimated for the parameter $\Delta Y/\Delta Z$). Models of massive AGBs can reach Y values of ~ 0.35 in their envelopes, and therefore models based on the formation of this high helium population out of massive AGBs ejecta can not reproduce the high Y values suggested by observations (Karakas et al. 2006). Similarly, models based on yields coming from either Type II or Type Ia supernovae (SNe Ia) are not successful (Romano et al. 2007; Marcolini et al. 2007; Choi & Yi 2008). Pumo et al. (2008) noticed that a very high helium content (Y up to ~ 0.38) can be achieved already just after the second dredge-up in the envelopes of the most massive super-AGB’ stars, as shown by the models by Siess (2007a). Super-AGBs are the stars that reach a carbon oxygen core mass of $\sim 1.05 M_{\odot}$, and ignite carbon in conditions of semi-degeneracy. The final outcome of this burning is a degenerate oxygen-neon core, that can now traverse a “normal” thermal pulse (TP) phase, like the stars with C-O core. A successful preliminary chemo-dynamical model, able to explain the helium distribution of the triple main sequence of NGC 2808, was then proposed in Paper I. We assumed that a “first” SG formed out of the ejecta of super-AGBs, so that this population has a very high Y, similar for all stars, while, as the SG formation phase proceeds, a “second” SG forms out of gas from massive AGBs mixed with pristine gas falling back onto the central regions and has a smaller helium content. This model produces a gap in the helium distribution of SG stars and can successfully reproduce the distinct populations identified in the color-magnitude diagram of NGC 2808.

To make further progress in understanding the origin of SG stars and to test the viability of different hypotheses

on the origin of the gas out of which SG stars formed, it is essential to explore whether all the chemical anomalies that characterize SG stars can be successfully reproduced. Unfortunately, only a few models of super-AGBs are available in the literature, and no low metallicity mass has been evolved through the whole TP phase. For the case of helium, we can rely on the helium abundance reached in the envelope after the second dredge up, as computed by Siess (2007a), but we do not know how precisely the other abundances will be modified by HBB during the rest of the stellar life, until the whole envelope is lost to the interstellar medium. In addition, even when the first models through the super-AGB TP phase will be available, their input physics must be carefully explored, as done for the massive AGB stars. Until then, we must make guesses on their yields. In this paper, we simply propose that the yields from super-AGBs for O, Na, Mg, Al, are compatible with the patterns observed in the most extremely anomalous GC populations. For instance, the sum of the CNO abundances can remain close to the initial value during the thermal pulse phase of super-AGBs, as they have a limited efficiency of third dredge up, because of the weak helium luminosity reached during the thermal pulses (Siess 2007b). We then *extrapolate* the yields computed for the lower AGB masses to the super-AGB regime. The extrapolation must satisfy two constrains: 1) super-AGBs have oxygen-neon core masses larger than the largest carbon-oxygen core masses of the most massive AGBs that do not ignite carbon. Consequently, we expect more extreme physical conditions in their convective envelopes, than in those of the most massive AGBs we have computed, and a more advanced nucleosynthesis due to proton-capture elements (this assumption also depends on the effect of mass loss, and on the total duration of the thermal pulse phase); 2) in addition, the results must not be in deep contrast with the observed abundance patterns. As for the effect of the third dredge up, in this work we will assume that dredge up in super-AGBs, if any, is less efficient than in less massive AGBs, as suggested by Siess (2007b).

2.2 Oxygen burning

One of the most challenging issues in modelling the abundance patterns of SG stars in globular clusters is the SG low oxygen abundance.

Population II stars are in general α -enriched, and thus oxygen-enriched, due to the role of SNII in the oxygen production (e.g. Matteucci & Greggio 1986); in order to deplete the abundance of oxygen, the gas from which SG stars are formed must have gone through the full CNO cycle (the ON chain) that occurs at temperatures of ~ 40 MK in the stellar interior, and needs temperature of $T_{\text{bce}} \sim 60 - 80$ MK at the bottom of AGB convective envelopes (T_{bce}), both due to the much lower stellar densities of these regions, and to the shorter evolutionary times of this phase (see, e.g. Prantzos et al. 2007).

Efficient ON burning occurs due to HBB in massive AGBs—and consequently in super-AGBs, due to the higher temperatures reached at the bottom of their convective envelopes. Ventura & D’Antona (2005a) showed that more efficient ON processing is favoured by more efficient convection. However, the most massive AGBs with values of the metallicity ($Z \sim 10^{-3}$) typical of the clusters showing very strong chemical anomalies, can not deplete oxygen by more than ~ 0.8 dex. Starting from a typical $[\text{O}/\text{Fe}] = +0.4$, the minimum oxygen abundance is $[\text{O}/\text{Fe}] \sim -0.35 - -0.40$. In most GCs the O-depletion is limited to $\lesssim 0.8$ dex, but we do know that giants in clusters like M 13 (Snedden et al. 2004) or NGC 2808 (Carretta et al. 2008) show extreme stars with oxygen depletion down to a factor larger than 20.

There are two options to explain the oxygen abundance of these extreme stars: 1) either the strong O-depletion is due to the higher T_{bce} reached by super-AGBs; 2) or it is a consequence of in-situ mixing in red giants (these extreme anomalies have been so far found only along the giant branch) suffering deep extra-mixing due to their very high initial helium content. Indeed, in these stars, the molecular weight barrier that could forbid deep mixing at luminosities below the red giant bump is much smaller than in stars with normal Y (D’Antona & Ventura 2007).

In both cases, if we wish to have an educated guess about the oxygen yield of super-AGBs, the choice is mandatory: it must be *smaller* than for the maximum computed AGB mass, so we adopt $[\text{O}/\text{Fe}] = -1.1$ for the progenitor largest mass $9 M_{\odot}$.

2.3 Sodium production

Understanding the sodium abundance in the SG stars presents similar complexities. The sodium yield is provided by three different stages of the life of a massive AGB star. At each of these stages, different problems must be attacked to determine the yields, and may have different solutions. In addition, during these stages an AGB star loses mass, so the total yield will also depend on the mass loss rate in each of these phases. We have discussed these problems in a series of papers dedicated to the nucleosynthesis in AGBs (Ventura & D’Antona 2008a, and references therein). Here below we outline the phases during which the sodium changes:

(1) The first phase during which sodium increases is when the second dredge up, before the star climbs up the AGB,

mixes to the surface the ^{23}Na and ^{22}Ne produced inside the star during the previous H-burning phases.

(2) Immediately after, the reaction $^{22}\text{Ne}(p,\gamma)^{23}\text{Na}$ takes place, due to the HBB, and ^{23}Na begins to be cycled back through the reaction $^{23}\text{Na}(p,\alpha)^{20}\text{Ne}$. The most important of these two paths in order to determine the total ^{23}Na yield is the first one, $^{22}\text{Ne}(p,\gamma)^{23}\text{Na}$, that, unfortunately, is uncertain *by a factor* ~ 2000 in the range of temperature of interest for oxygen depletion (Hale et al. 2002). It is important to point out, however, that, once all the ^{22}Ne is burned to ^{23}Na via HBB, the sodium production does not increase even if we further increase the cross section of this reaction (Izzard et al. 2007). We can keep more sodium only by lowering the reaction rate $^{23}\text{Na}(p,\alpha)^{20}\text{Ne}$ (Ventura & D’Antona 2006).

(3) The third stage by which sodium in the envelope changes is the third dredge up phase (3DU) following each thermal pulse. The smaller the initial mass, the more effective the 3DU becomes. At each episode, the 3DU in fact mixes down into the helium layers the nitrogen obtained in the H-envelope due to HBB-CN cycling of the ^{12}C produced during the thermal pulse and partially dredged up. Consequently, *primary* ^{22}Ne , produced by the chain $^{14}\text{N}(\alpha,\gamma)^{18}\text{F}(\beta^+,\nu)^{18}\text{O}(\alpha,\gamma)^{22}\text{Ne}$, is also dredged up from the helium inter-shell, and is converted into primary sodium by HBB. If the stars go through many episodes of 3DU, this third phase can increase the sodium abundance even by orders of magnitude, but it also leads to a strong increase in the total C+N+O yield (see sect. 2.4) which has not been observed in globular clusters.

All the computations of AGB evolution in the literature clearly show that, as the AGB mass increases, the sodium yield decreases; this is a consequence of the increasing T_{bce} . A larger T_{bce} depletes more oxygen, and destroys sodium more easily by the $^{23}\text{Na}(p,\alpha)^{20}\text{Ne}$ cycle. In addition, in smaller masses the 3DU will dredge up more the ^{22}Ne and convert it into sodium. This implies that the massive AGB models, and probably the more massive super-AGBs as well, provide a *direct* O-Na correlation, and not the observed anti-correlation. We address this problem in sect. 5.1 and show the possible role played by dilution with pristine gas in turning this correlation into the observed Na-O anti-correlation.

In order to reproduce the observed abundances of Na in the SG, we need to have *the largest possible sodium yields for the masses in which the 3DU does not play a strong role*, that are, as we will see from the C+N+O examination, $M \gtrsim 5 M_{\odot}$. Starting from the reference values of the yields from the calculation of Ventura & D’Antona (2009) (see their Table 2 and Table 1), there are two key ingredients which are still affected by significant uncertainties and could lead to larger sodium abundance in the massive AGB envelopes:

(i) **the $^{20}\text{Ne}(p,\gamma)$ reaction rate:** a 50 % increase in the $^{20}\text{Ne}(p,\gamma)$ rate is well within the NACRE (Angulo et al. 1999) reaction rate uncertainties and, keeping all other parameters fixed, will lead to a 0.15 dex increase in the sodium yield, because the equilibrium of the Ne-Na chain is shifted towards ^{23}Na ;

(ii) **the ^{20}Ne abundance:** the initial ^{20}Ne abundance is not well known², and it may also vary from cluster to cluster (sect. 6). In our reference computation, the ^{20}Ne abundance is already α -enhanced, as for oxygen and the other α -elements, by 0.4 dex with respect to the solar ratios. If we increase this initial ^{20}Ne by another factor 2, the final $[\text{Na}/\text{Fe}]$ is increased by ~ 0.2 dex (for the important masses from 6.3 to 5 M_{\odot}). Owing to our numerical tests, in a first approximation we can assume:

$$\delta[\text{Na}/\text{Fe}] \simeq \delta[^{20}\text{Ne}/\text{Fe}] \quad (1)$$

If we adopt both the enhanced reaction rate and the larger ^{20}Ne abundance, the combined effect of these two assumptions leads to $[\text{Na}/\text{Fe}] = [\text{Na}/\text{Fe}]_{\text{standard}} + 0.35$. In our calculations the increase of the sodium yield is calibrated by comparison with the observational data by +0.3dex (see Table 1 and Fig. 1) for the masses up to 6 M_{\odot} . For the super-AGB stars, we decrease the sodium content to $[\text{Na}/\text{Fe}] = 0.45$, based on the hypothesis that these stars will be more efficient in destroying sodium. We warn that this suggestion will need confirmation from real computation of super-AGB evolution. Once we have assumed a "standard" table of abundances with increased sodium, we still can use equation 1 to model clusters with abnormally larger α -elements abundances (see the case of M4 in sect. 6.2)

2.4 The total CNO abundance in the SG

For C, N and O we will use the yields from Table 2 of Ventura & D’Antona (2009) without any adjustment. For the masses from 6.5 to 9 M_{\odot} , the super-AGB regime, we adopt the C and N envelope abundances of the most massive computed AGB model of 6.3 M_{\odot} . The O abundance in this mass range, instead, has been calibrated to fit the abundance of the O-poor stars present in NGC 2808, as discussed in the previous subsection (cf. Fig. 1).

As most of the SG stars in GCs do not show a significant increase of the total CNO (Ivans et al. 1999, 2001; Carretta et al. 2005), the matter out of which the SG forms can not come from stars in which the effect of the 3DU is relevant. A reasonable assumption based on the data is that the total CNO in most clusters so far examined is within a factor two of the CNO of the FG. If we adopt the yields from Ventura & D’Antona (2009) as our reference values, and assume that SG stars form only from pure AGB ejecta, the limiting mass for the SG formation is then $\sim 5 M_{\odot}$, and the limiting age ~ 100 Myr (time evolution of the 5 M_{\odot} , see Table 1). If, on the other hand, the matter from which SG stars form is diluted with pristine gas, as shown to be necessary in sect. 5, the limiting age for SG formation can be a bit larger.

An interesting indication concerning possible variations in CNO comes from recent spectroscopic observations of a few red giants in NGC 1851. These observations have shown

that the C+N+O abundance of the stars observed varies by up to a factor 4 (0.6 dex, Yong et al. 2009). In addition, new HST photometric data (Milone et al. 2008) have revealed a split subgiant branch. Two interpretations are possible: either the stars in the lower subgiant branch are older by ~ 1 Gyr (Milone et al. 2008), or they are SG stars with a larger total C+N+O content (Cassisi et al. 2008). Ventura et al. (2009) show that the total C+N+O must be about a factor three larger in the lower subgiant branch stars. They argue that the matter from which the SG formed should have been diluted at 50% with pristine matter having approximately the composition of the ejecta of $\sim 4 M_{\odot}$ AGBs. With this choice, they can explain at the same time the C+N+O abundance and the lack of a significant helium enrichment, that would be recognized in the luminosity of the blue horizontal branch stars (Salaris et al. 2008). In our scenario, the SG in this case should have formed from matter collected in the cluster until an age of ~ 150 Myr, at the evolution of the 4 M_{\odot} (Ventura et al. 2009).

In the construction of possible models for the SG, then, the C, N and O composition of the SG is an important parameter, and it is also important to obtain further observations of its range of variability for as many clusters as possible. We point out that the AGB models of Ventura & D’Antona (2009) adopted here have smaller CNO enhancement than other published models (e.g. Karakas & Lattanzio 2007), as they have a smaller number of TPs and 3DU episodes. This is due both to the mass loss rate adopted and to the use of an efficient convection model that provides a larger stellar luminosity (and consequently a larger mass loss rate) for a fixed core mass. Should we adopt models with a more efficient 3DU, or a larger number of TPs, the formation of the SG must occur at shorter age (larger evolving initial masses) both for the "normal" SG clusters (no CNO enrichment) and for clusters like NGC 1851, where the CNO enrichment is present.

2.5 The Magnesium and Aluminium yields

In some (massive) GCs only, also an anticorrelation between magnesium and aluminium is revealed. The depletion in total Mg is restricted to 0.2 – 0.4 dex. Generally, the stars with the highest degree of oxygen depletion are also strongly enriched in Al, up to the values $[\text{Al}/\text{Fe}] \sim 1 - 1.2$ found in the red giants of M13 and M15 (for a summary of the data of the last decade, see Ivans et al. 1999). The anticorrelation shows that the matter of the SG has been subject to the Mg–Al chain, that, favouring proton captures by the heavy isotopes of magnesium, eventually leads to the synthesis of ^{27}Al (Denissenkov & Herwig 2003; Ventura & D’Antona 2005a). In models with many third dredge up episodes, penetration of the convective envelope into the layers touched by 3α burning may bring to the surface ^{25}Mg and ^{26}Mg synthesized via α captures on ^{22}Ne nuclei. These isotopes produce ^{27}Al by proton capture, once the H-shell is reactivated (Ventura & D’Antona 2008b). The recent analysis of Mg and Al abundances from UVES spectra in 18 GCs, by Carretta et al. (2009b), shows however large cluster to cluster variations in the Al–Mg anticorrelation, and that in most cases the Mg variation is very limited, even for stars with $[\text{Al}/\text{Fe}] \sim 0.8$. They also show that the maximum Mg abundance and the minimum Al abundance (that should be

² In recent years, an increase in the ^{20}Ne abundance for the Sun has been suggested, as it could produce the opacity increase necessary to obtain a better fit of the solar oscillation spectrum, once the iron and oxygen content are reduced following the results of the 3D analysis of the solar spectrum (for a summary of this complex problem, see Asplund et al. 2009).

indicative of the composition of the FG) may be significantly different in different clusters –even by an order of magnitude for Al. Where the Mg abundance is larger than the typical $[\text{Mg}/\text{Fe}]+0.4$ assumed for the α -enhanced composition, this may reflect different overabundances in the matter forming the FG, and we must take it into account, both for magnesium and for the other α elements (see sect. 6.2).

In their theoretical study, Ventura & D’Antona (2008b, 2009) adopted the NACRE upper limits for the aluminium production from proton captures on ^{25}Mg and ^{26}Mg , in order to obtain very significant Al production in their massive AGB models. Their aim was to reproduce the extended Mg–Al anticorrelation present in the M13 and M15 red giants. Their results, however, are in contrast with the abundance patterns in M4 (NGC 6121) in which the maximum $[\text{Al}/\text{Fe}]$ is ~ 0.8 , and the *minimum* is $[\text{Al}/\text{Fe}] \sim 0.6$ (Ivans et al. 1999; Marino et al. 2008a), so that this cluster does not show great Al variations, if any.

As the large Al abundances of NGC 2808 seem to refer only to very oxygen poor stars, we can attribute them to the super-AGB evolution. Consequently, we decided to restore the above cross section to their standard values, and assume that significant Al production is limited to the super-AGB masses only. For the temperatures of interest here ($T \sim 10^8\text{K}$), the NACRE recommended values for the $^{25}\text{Mg}(p,\gamma)^{26}\text{Al}$ and $^{26}\text{Mg}(p,\gamma)^{27}\text{Al}$ reactions are smaller, respectively, by a factor of 2 and 4 than the rates adopted by Ventura & D’Antona (2009). The aluminium production is consequently reduced: its average content in the ejecta of massive AGBs of 5 and $6M_{\odot}$ with metallicity $Z=0.001$ diminishes to $[\text{Al}/\text{Fe}]=0.7$ and 0.62 when the recommended cross sections for the proton capture reactions by magnesium isotopes are adopted, to be compared to the published values of $[\text{Al}/\text{Fe}]=1.02$ and 1.04 . The modifications to the Mg and Al abundances are provided in Table 1.

3 GENERAL ASSUMPTIONS OF THE MODEL

The general assumptions driving the present models are the same adopted in Paper I, and we recall them here briefly. We assume that the FG stars are already in place and have the same chemical abundances of the pristine gas from which they form. The SG stars form from AGB ejecta. In order to have a current similar number of SG and FG stars, the FG population must have been initially about ten times more massive so as to supply enough mass in AGB ejecta to form a sizable SG population. This conclusion remains substantially valid even if, during its evolution, the GC accretes some external pristine gas. A very large initial FG is invoked also by Renzini (2008) on the basis of the large amount of helium observed in some multiple populations of very massive GCs (see sect. 2.1).

We assume that only SG stars with $M \leq 9 M_{\odot}$ can form (cf. Paper I). More massive stars explode as SNe II, but the very small spread of iron in GCs (c.f. Carretta et al. 2009a) indicates that the SG stars hardly have been polluted by SNe II (we discuss this point in the Introduction and in sect. 7). Moreover, as shown in sect. 6, the AGB pollution takes tens of Myr to produce the observed chemical patterns; as the first SNe II starts to explode after ~ 5 Myr, they would vent away all the gas, preventing the formation of a

substantial amount of SG stars³. Given a Kroupa initial mass function (IMF) with an upper mass of $9 M_{\odot}$, the mass of the long-lived ($M \lesssim 0.8 M_{\odot}$) SG stars is 54% of the total forming SG population.

4 COMPUTATIONAL METHOD

The computational framework adopted for this study is based on a one-zone model for globular clusters in which the evolution of AGB ejecta and pristine gas - from which SG stars form - is regulated by a few parameters. The variation of these parameters can be easily controlled and this allows us to explore their relative importance on the resulting SG chemical properties.

The evolution of the gas and the process of SG formation is modelled by the following equations which are integrated by means of a fourth-order Runge-Kutta method:

$$\dot{\rho}(t) = \alpha \rho_{*,\text{FG}} + \dot{\rho}_{\text{pr}}(t) - \nu \frac{\rho(t)}{t_{\text{sf}}} \quad (2)$$

$$\dot{\rho}_{\text{ch}}^{\text{k}}(t) = \alpha^{\text{k}} \rho_{*,\text{FG}} + \beta^{\text{k}} \dot{\rho}_{\text{pr}}(t) - \nu \frac{\rho_{\text{ch}}^{\text{k}}(t)}{t_{\text{sf}}} \quad (3)$$

$$\dot{\rho}_{\text{pr}}(t) = \frac{\rho_{0,\text{pr}}}{\sqrt{\pi}\tau} \exp -[(t - t_{\text{ac}})/\tau]^2 - \nu \frac{\rho_{\text{pr}}(t)}{t_{\text{sf}}} \quad (4)$$

$$\dot{\rho}_{*,\text{SG}}(t) = \nu \frac{\rho(t)}{t_{\text{sf}}} \quad (5)$$

Here below we discuss each of the above equations:

Eq. 2 - This equation describes the time evolution of the total gas density ρ . The first term in the right hand side (RHS) represents the increment of ρ due to the gas lost by the dying stars. In principle, we would take into account the mass return from the FG stars as well as from the newly formed SG stars. These latter, however, are much less than the former, and we neglect their contribution. We thus consider only the density $\rho_{*,\text{FG}}$, and the specific mass return rate is given by $\alpha = \dot{\rho}_{*,\text{FG}}/\rho_{*,\text{FG}}$; this rate is computed following Ciotti et al. (1991) (see their eq. 3), adapted to the Kroupa IMF adopted here. The second term in the RHS of eq. 2 takes into account the gas increment due to the accretion of the pristine gas whose density is ρ_{pr} . Finally, the last term describes the reduction of gas because of the star formation, and is characterized by the SF efficiency ν and the SF timescale t_{sf} . The former is a free parameter summarizing our uncertainties about star formation and with values in the range $0 < \nu < 1$; the latter coincides with the free-fall time, and is thus proportional to $(\rho^{-1/2})^4$.

³ On the contrary, massive stars in the FG must be present for two reasons. First, as the FG is initially nearly ten times larger than today (in order to deliver enough ejecta to form the observed amount of SG), SN explosions allow the cluster to get rid of the mass excess in a time shorter than the Hubble time (cf. Paper I); second, Extreme, very O-poor stars present in some cluster (e.g. NGC 2808) can arise only from a pure AGB ejecta, and this could not be possible without the previous action of the FG SNe II clearing initially the GC of its residual pristine gas.

⁴ In a full hydrodynamic treatment, as in Paper I, t_{sf} is defined as the maximum between the local cooling time and the local free-fall time, but the first one is usually much shorter

Eq. 3 - Besides the total gas density, it is necessary to evaluate the density of the single chemical elements we are interested in. In our models we take into account the abundance evolution of nine elements: He, Li, C, N, O, Na, Mg, Al, Fe. Equation 3 represents a system of $kmax = 9$ equations, each modelling the evolution of the density ρ_{ch}^k of the k -th element. In these equations $\alpha(t)^k$ and β^k represent the mass return rate of the k -th element in the FG, and the mass fraction of the k -th element in the pristine gas, respectively. The latter is determined by the assumed initial chemical composition of the pristine gas, while the values of $\alpha(t)^k$ are obtained at each time by the interpolation of the values given by our adopted ejecta abundances (cf. Fig. 1 and Table 1).

Eq. 4 - This equation describes the evolution of the pristine gas density ρ_{pr} . The two terms on the RHS model the time evolution of the pristine gas accretion (first term) and the SG star formation (second term). The gaussian form adopted to model the pristine gas accretion is arbitrary, but allows us to easily explore different accretion scenarios. The time t_{ac} regulates the time at which the maximum accretion rate occurs, and the time τ controls how the accretion evolves: a small value of τ corresponds to a sudden accretion, while a large value gives rise to a more gradual growth. Finally, the constant $\rho_{0,pr}$ controls the amount of available pristine gas. The three constants t_{ac} , τ and $\rho_{0,pr}$ must be regarded as free parameters of our models.

Eq. 5 - Finally, equation 5 regulates the growth of the SG stellar population.

In addition to $\rho_{0,pr}$, ν , t_{ac} , τ , one more parameter must still be added: the time t_{end} at which the simulations stop. It regulates not only the amount of SG stars formed, but also their overall chemical distribution, as the chemical abundances of the FG ejecta vary in time (cf. Fig. 1). Its value is constrained by the observational evidence (discussed in sect. 2.4) that the sum of CNO elements varies no more than a factor two among the GC stars (Cohen & Meléndez 2005) (or by a factor three in NGC 1851, see Ventura et al. 2009); this implies that the SG progenitors must be AGB stars with masses larger than $\sim 5 M_{\odot}$ ($\sim 4 M_{\odot}$ in the latter case) and that the SG formation can not continue longer than the lifetime of these stars, that is $t_{end} \lesssim 100$ Myr (or $\lesssim 150$ in the latter case)⁵ (cf. Fig. 1 for the behaviour of C+N+O with time).

Finally, we introduce the ratio $x = \rho_{*,SG}^n / \rho_{*,tot}^n$ between the SG stars and the total nowadays alive stars $\rho_{*,tot}^n = \rho_{*,FG}^n + \rho_{*,SG}^n$. Its current value depends not only on the duration and efficiency of the SF of the SG stars, but also on the subsequent loss of FG stars (see Paper I). We point out that this parameter does not enter directly into the models (it is in fact absent in eqs. 2-5); its value is inferred *a posteriori* for a more realistic fit of the data. We will return on this point in sect. 6, when comparing our models to specific GCs.

In the end, we summarize in Table 2 the key parameters (besides the chemistry of the AGB ejecta) characterizing our models.

Table 2. Parameters characterizing the models

t_{ac}	time of maximum accretion of pristine gas
τ	time scale of the pristine gas accretion
t_{end}	time marking the end of the SG formation phase
$\rho_{*,FG}$	density of the FG stars
$\rho_{0,pr}$	density regulating the amount of available pristine gas
ν	SF efficiency
x	the ratio between the nowadays alive SG and total stars

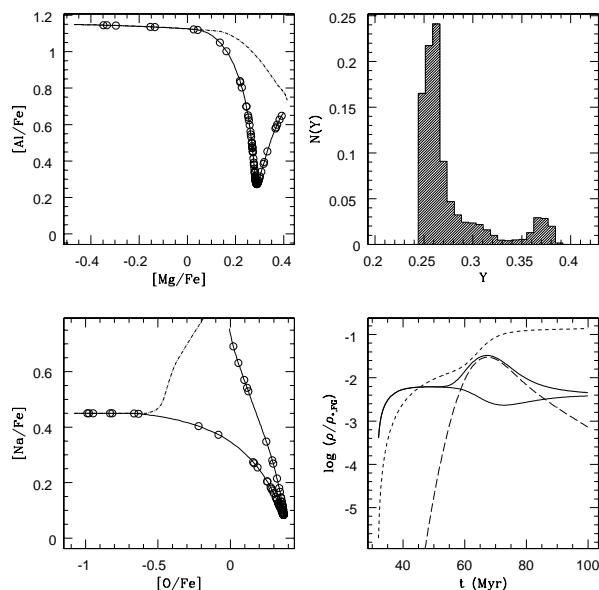


Figure 2. Top-left panel: chemical evolution of the RM in the plane $[Mg/Fe]$ - $[Al/Fe]$. Bottom-left panel: chemical evolution of the RM in the plane $[O/Fe]$ - $[Na/Fe]$ plane. In these panels the dot-dashed line represents the ISM chemical pattern of the model without accretion of pristine gas (RMNOPG), while the solid line holds for the RM, in which the accretion occurs; the open circles represent a statistical sampling of the SG stars. Top-right panel: helium distribution function of the SG stars. Bottom-right panel: evolution of the total amount of ISM (bold solid line), AGB ejecta (solid line), pristine gas (long-dashed line) and SG stars (short-dashed line).

5 MODEL ANALYSIS

5.1 The reference model

To illustrate how our model works, we focus our attention on a model with the following parameter set $(t_{ac,7}, t_{end,7}, \tau_7, \rho_{0,pr}, \rho_{*,FG}, \nu, x) = (6.5, 10, 0.6, 15, 150, 0.5, 1)$, where the times are expressed in 10^7 yr and the densities in $M_{\odot} \text{ pc}^{-3}$. Note that we here are interested only in the evolution of the SG stars, and we set $x = 1$. We checked that the current choice of parameters gives (in absence of the accretion of pristine gas) the same temporal profile of the gas and of the SG stars of the reference model of Paper I (cf. its Fig. 2); for this reason, we’ll refer to the one zone model described in this section as the reference model (RM). We consider an amount of available pristine gas one tenth of the FG mass, nearly a factor two larger than that of the ejecta delivered after $\sim 10^8$ yr.

⁵ A possible mechanism able to clear the ISM in a globular clusters in this lapse of time is given by the explosions of type Ia supernovae (see Paper I).

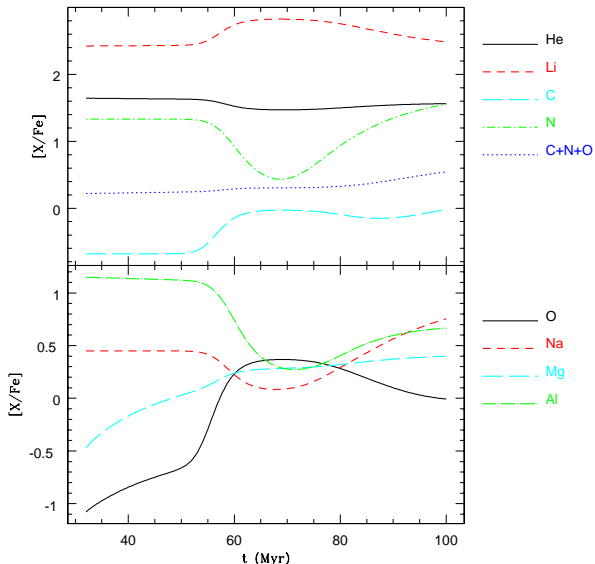


Figure 3. Time evolution of the chemical abundances in the ISM of the RM.

The main properties of this model are shown in Fig. 2. The two left panels illustrate the chemical path of the model in the planes $[\text{Al}/\text{Fe}]$ - $[\text{Mg}/\text{Fe}]$ and $[\text{O}/\text{Fe}]$ - $[\text{Na}/\text{Fe}]$. The top-right panel provides the helium distribution function (hereafter HDF) of the SG stars, while the bottom-right panel shows the time evolution of the amount of several quantities. Initially, only gas returned by the FG stars is present (thin solid line). Later on, the total gas content (thick) first experiences a “jump” as a consequence of the pristine gas (long-dashed line) accretion, and successively decreases because of the star formation. The amount of SG stars (short-dashed line) shows, as expected, a rapid increase in conjunction with the accretion.

Figure 3 illustrates the abundance evolution of different elements in the ISM of the RM. A comparison of Fig. 1 and Fig. 3 clearly shows that, as anticipated in sect. 2.2, the presence of pristine gas is necessary in order to reproduce the O-Na anticorrelation observed in all the GCs. In Fig. 1 the O and Na abundances in the FG stellar ejecta grow simultaneously, and no anticorrelation between these two elements can be established; on the other hand, Fig. 3 clearly indicates how the pristine gas accretion produces opposite slopes in the time evolution of the O and Na abundances in the ISM, thus producing an anticorrelation similar to that observed in globular clusters.

This point is illustrated even more vividly in the bottom-left panel of Fig. 2. This panel includes the chemical path of the gas *in absence of any accretion* (i.e. $\rho_{\text{pr}} = 0$), represented by the dot-dashed line. This model (hereafter the RMNOPG model) starts from the O-poor end of this line since the ejecta of the most massive AGBs are assumed to be particularly deprived of oxygen (see Fig. 1 and the discussion in sect. 2). As gas from less massive AGB stars contributes to the ISM both the abundances of Na and O increase giving rise to a correlation rather than the observed anticorrelation. The path followed by the RM when the effect of pristine gas accretion is included clearly illustrates

the role of this gas in establishing the Na-O anticorrelation. Since the ISM is initially composed only by AGB ejecta, the RM track initially coincides with that of the model with no pristine gas. At $t \sim 55$ Myr, when $[\text{O}/\text{Fe}] \gtrsim -0.5$, the amount of the infalling pristine gas becomes substantial, and the RM moves “downward” at increasing values of $[\text{O}/\text{Fe}]$, giving rise to a $[\text{O}/\text{Fe}]$ - $[\text{Na}/\text{Fe}]$ anticorrelation. This motion is not uniform because the pristine gas accretion suddenly increases (decreases) the abundance of oxygen (sodium), “pushing” the model in short time towards higher (lower) values of $[\text{O}/\text{Fe}]$ ($[\text{Na}/\text{Fe}]$) (cf. Fig. 3). As the amount of pristine gas in the ISM increases, the trajectory moves toward its minimum located at $[\text{O}/\text{Fe}] = 0.37$ and $[\text{Na}/\text{Fe}] = 0.1$ dex, “above” the point identified by the ratios $[\text{O}/\text{Fe}] = 0.4$ and $[\text{Na}/\text{Fe}] = 0$ of the pristine gas. Successively, the accretion rate of the pristine gas reduces becoming lower than the SFR, and the relative amount of this gas in the ISM decreases more and more. The ISM composition evolves back toward the chemical abundance of the AGB ejecta and the chemical path of this model tends again toward that of the RMNOPG model.

It is important to point out that the ISM trajectory in the Na-O plane is not sufficient to predict the distribution of SG stars in this plane. In fact, such a path is, in a sense, similar to a stellar Color-Magnitude diagram in which some regions are more populated than others owing to the longer time spent there by the stars. In our model the amount of SG stars along a certain portion of the chemical trajectory depends on the rate of evolution of the ISM chemical abundance as well as on the SFR (which is proportional to $\rho^{3/2}$). In order to show how the $[\text{O}/\text{Fe}]$ - $[\text{Na}/\text{Fe}]$ and $[\text{Mg}/\text{Fe}]$ - $[\text{Al}/\text{Fe}]$ diagrams are actually populated by the SG stars, in Fig. 2 we have plotted twenty open dots representing a statistical sampling of the SG stars forming along the chemical path. Consider, for instance, the diagram $[\text{O}/\text{Fe}]$ - $[\text{Na}/\text{Fe}]$: only a few stars populate the two branches of the curve, while most of them form close to its cusp; the cusp coincides with the maximum amount of ISM and the consequent maximum SFR. Although the time spent by the model along the two branches is similar (cf. Fig. 3 and the bottom-right panel of Fig. 2), the descending one is more populated by stars because the ISM density and the SFR are larger at this stage.

Finally, the top-right panel of Fig. 2 shows the HDF. A small number of stars (10%) have an helium abundance $Y > 0.35$. These stars coincide with the most O-poor stars present in the $[\text{O}/\text{Fe}]$ - $[\text{Na}/\text{Fe}]$ diagram. The stars giving rise to the peak around the range $0.24 < Y < 0.29$ form when the maximum amount of pristine gas is present in the GC, and correspond to the stars populating the region around the cusp. The tail at $Y \sim 0.3$ is composed by stars formed during two nearly chemically “symmetric” phases, just before and after the occurrence of the bulk of the pristine gas accretion (cf. Fig. 3)).

5.2 Exploring the parameter space

We now explore the dependence of the model on the chosen set of parameters through variations of the chemical paths in the $[\text{O}/\text{Fe}]$ - $[\text{Na}/\text{Fe}]$ plane and variations of the HDF. We consider several models, each differing from the RM in the value of a single parameters. All the models are listed in Table 3.

Table 3. Models adopted for the exploration of the parameter space.

Models	$t_{\text{ac},7}$	τ_7	$t_{\text{end},7}$	ρ_{pr}	$\rho_{*,\text{FG}}$	ν	panel and style ^c
RM	6.5	0.6	10.0	15	150	0.5	all, solid, black
RMNOPG				0.0			all, dot-dashed, green
RMMPRM				4.5			a, dashed, blue
RMMPRM				45			a, dotted, red
RMTACL	5.0						b, dashed, blue
RMTACM	8.0						b, dotted, red
RMTAUL		0.3					c, dashed, blue
RMTAUM		1.2					c, dotted, red
RMEFFL						0.1	d, dashed, blue
RMEFFM						1.0	d, dotted, red
RMTNDL			7.0				e, dashed, blue
RMTNDM			13.0				e, dotted, red
RMFGDL				1.5	15		f, dashed blue
RMFGDM				150	1500		f, dotted, red
RMTSFL						0.0 for $t_7 < 5$ 1.0 for $t_7 \geq 5$	dashed, blue ^d
RMTSFM						0.0 for $t_7 < 7$ 1.0 for $t_7 \geq 7$	dotted, red ^d

^aTimes are given in 10^7 yr and densities in $M_{\odot} \text{pc}^{-3}$.

^bFor each model only the parameter values differing from the RM are reported, all the others being the same.

^cThis column indicates the panels of Figs. 4 and 5 in which the single models are shown, and their line style.

^dReferred to Fig. 6.

5.2.1 The $[O/Fe]$ - $[Na/Fe]$ diagram

The six panels in Fig. 4 illustrate how changes of each single parameter affect the RM behaviour in the $[O/Fe]$ - $[Na/Fe]$ diagram. The RM path (solid line) is replicated in every panel to facilitate the comparison with the different modified models. For the same reason we also include in all the panels the dot-dashed line representing the behaviours of the RMNOPG (see Fig. 2). We now discuss these panels.

Panel a - In this panel the RM is compared with two similar models, but with $\rho_{\text{pr}} = 4.5 M_{\odot} \text{pc}^{-3}$ (RMMPRM, blue dashed line) and $\rho_{\text{pr}} = 45 M_{\odot} \text{pc}^{-3}$ (RMMPRM, red dotted line). The O-poor branch of the RMMPRM substantially overlaps the analogous RM branch as long as the amount of accreted pristine gas is relatively low in both models. The rising branch, instead, is shifted toward lower values of $[O/Fe]$. This shift is a consequence of the smaller amount of pristine gas, and its lower influence on the chemical abundance of the ISM; the dashed line tends to return more rapidly toward the dot-dashed one. The reduced value of ρ_{pr} affects the position of the cusp, which occurs at $[O/Fe]=0.3$ and $[Na/Fe]=0.2$ earlier than in the RM model.

Also in this case the stars (open blue squares) form mainly around the cusp, but the two branches are more populated. This is due to the combined effect of the lower amplitude of the gaussian accretion rate and the dependence of the SFR on $\rho^{3/2}$; the result is a less marked peak in the SFR occurring at the cusp.

Similar considerations apply to the RMMPRM. While the descending branch overlaps again with those of the previous models, the cusp of the red dotted curve is located at a value of $[Na/Fe]$ nearly 0.2 dex lower than that of the blue curve, and the rising branch is shifted toward higher values of $[O/Fe]$. Finally, in this model the stars (open red triangles) are essentially all concentrated around the cusp.

Panel b - The models represented here are similar to the

RM, but with $t_{\text{ac},7} = 5$ (RMTACL, blue dashed line) and $t_{\text{ac},7} = 8$ (RMTACM, red dotted line). The O-poor descending branch of the dashed line is essentially similar to that of the RM, but slightly shifted toward lower values of $[Na/Fe]$; this is a consequence of the earlier accretion of pristine gas. The rising branch is instead longer and strongly shifted toward lower values of $[O/Fe]$ because at this stage the amount of pristine gas eroded by the SF is larger than in the RM. The dashed line tends therefore to reconnect earlier to the RMNOPG chemical pattern.

Given the delay in the gas accretion, the RMTACM follows the RMNOPG track for a longer interval, then quickly converges toward the cusp. The dotted rising branch is shorter and shifted toward higher values of $[O/Fe]$ for opposite reasons relative to the RMTACL.

Because of the delay in the accretion, the RMTACM descending branch is more populated by stars than the rising branch, while the opposite happens for the RMTACL. Once more, this is due to the fact that the SFR grows with the gas density. Note the gap in the stellar distribution along the descending dotted branch (open triangles). Initially, the RMTACM has enough time to form a substantial amount of AGB ejecta before the accretion becomes significant. A non negligible fraction of O-poor stars can thus form. The subsequent accretion moves the model toward the cusp very rapidly, and very few stars can be produced during this stage.

Panel c - In this panel the models with $\tau_7 = 0.3$ (RMTAUL, blue dashed line) and $\tau_7 = 1.2$ (RMTAUM, red dotted line) are compared. Smaller values of τ correspond to a more rapid accretion. The two lines are rather similar, but with the dotted rising arm being shorter and shifted toward O rich values; in this case, in fact, the longer duration of the accretion produces a more persistent influence on the RMTAUM which thus shows some delay in its tendency to reconnect with the RMNOPG line.

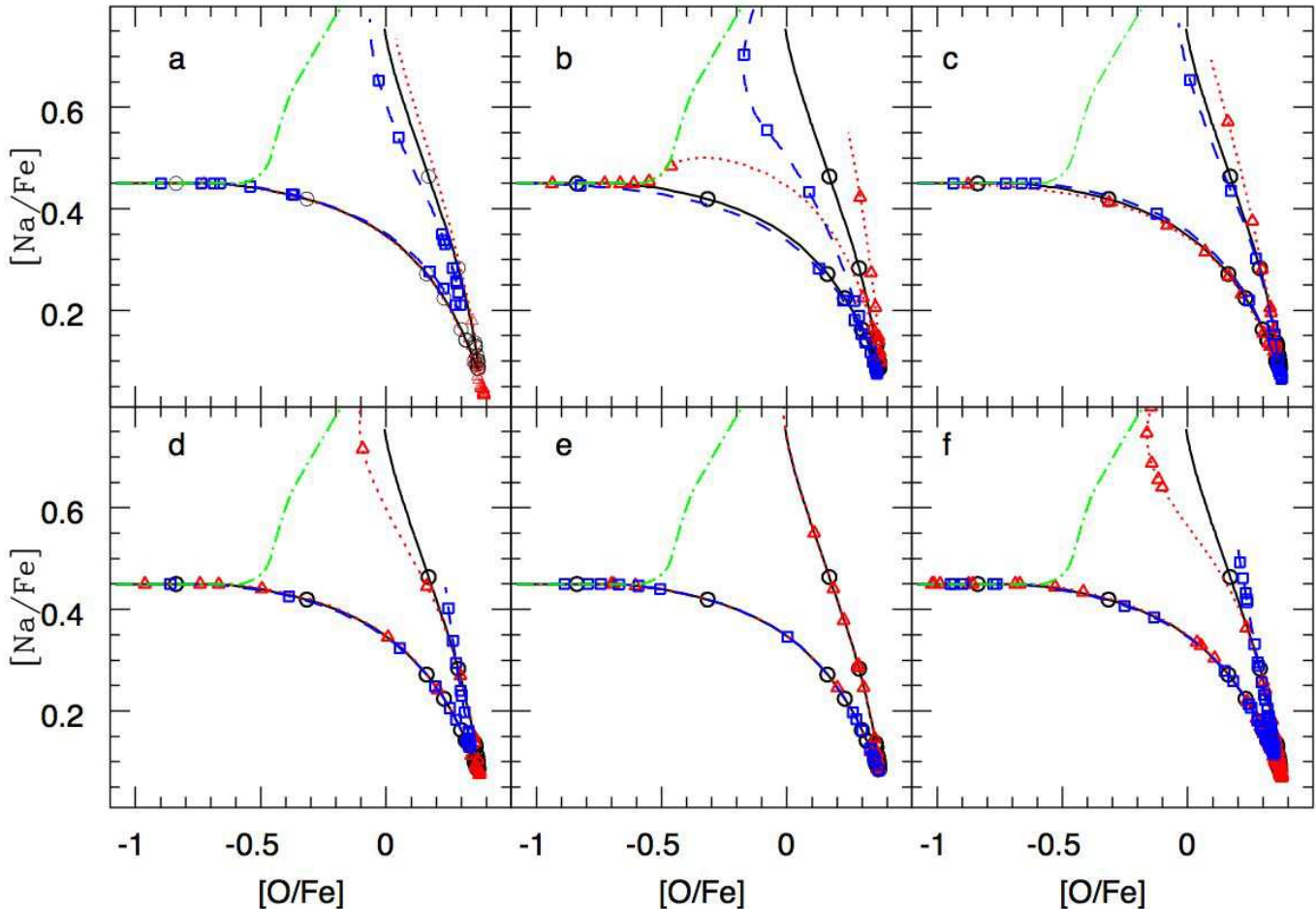


Figure 4. Chemical paths of models with modified parameters with respect to the RM. Each panel highlights the effect of a single parameter (see the text for more details). For practicality's sake, the RM (black solid line) and RMNOPG (green dot-dashed line) are reported in all panels. The different symbols represent statistical samples of the SG stars in different models.

The distributions of the stars along the dashed and dotted lines are also similar. However, a prevalence of O-poor stars in the RMTAUL (open squares) is present; owing to the shorter extent of the accretion, a larger amount of AGB ejecta can be initially collected without being significantly diluted by the pristine gas.

Panel d - The effects of the SF efficiency are investigated by models with $\nu = 0.1$ (RMEFFL, blue dashed line) and $\nu = 1$ (RMEFFM, red dotted line). As usual, the descending branches essentially overlap. The rising RMEFFM arm, instead, is more extended and shifted toward lower O abundances because the larger SF efficiency leads to a more rapid consumption of the ISM in general, and of the pristine gas in particular; once the bulk of the accretion is finished, the fresh AGB ejecta is diluted by a lower amount of the pristine gas still present in the ISM, and the RMEFFM chemical pattern moves more quickly toward the RMNOPG track.

Panel e - In all the previous models, we assumed $t_{\text{end},7} = 10$. Obviously, the duration of the SG formation phase may be different, and we studied the influence of such a duration on the chemical path of the SG stars. In this panel we show a model with $t_{\text{end},7} = 7$ (RMTNDL, blue dashed line) and a model with $t_{\text{end},7} = 13$ (RMTNDM, red dotted line).

As expected, the chemical paths coincide, but with the dotted one obviously longer than the dashed one. As the two models are identical, the number of stars formed along the common tracks is the same, and one could expect the same distribution of triangles and squares on them. Instead, it is apparent that the triangles are less than the squares on the first branches; this is due to the fact that the number of symbols indicating the stars is not proportional to the total number of stars actually formed; rather, for every model we adopt twenty symbols to represent the total number of SG stars in it, no matter if this number is different in different models. In particular, the two models shown in this panel are identical, and the same number of stars is formed along the descending branches; however, the RMTNDM lasts longer, and many more stars are formed along the rising branch. For this reason more triangles are distributed on this branch and less on the descending one, where the squares are more numerous.

Panel f - In this panel we show the behaviour of two models having both the values of $\rho_{*,\text{FG}}$ and ρ_{pr} ten times lower (RMFGDL, blue dashed line) and ten times higher (RMFGDM, red dotted line) than in RM. In sect. 5.1 we have justified our choice of $\rho_{*,\text{FG}} = 150 \text{ M}_{\odot} \text{ pc}^{-3}$; this choice,

however, although reasonable, remains arbitrary. We expect that our results depend on a scaling of $\rho_{*,\text{FG}}$ and ρ_{pr} , even if their ratio, and thus the relative amount of dilution due to the pristine gas, remains the same; in fact, a lower (higher) density of $\rho_{*,\text{FG}}$ produces a lower (higher) density of the AGB ejecta which, together with a lower (higher) ρ_{pr} , determine a lower (higher) SFR and a different evolution.

This difference is apparent in the present panel. As usual, also the two models shown here have very similar descending branches, but the RMFGDL cusp occurs at a higher value of $[\text{Na}/\text{Fe}]$. This is because, owing to the lower SFR in this model, less ejecta are initially subtracted by the star formation, and the dilution by the pristine gas is less effective. Successively, however, always because of the lower SFR, the pristine gas is depleted more slowly, remaining longer in the ISM and leading to a shorter rising branch. Opposite arguments hold for the RMFGDM, whose cusp is “deeper” and whose rising branch is longer. Note also that this arm is strongly bent “to the left” because, given the larger amount of ejecta (relative to the pristine gas) in this case, this model tends more quickly toward the RMNOPG.

5.2.2 The helium distribution function

Another crucial output of the models are the stellar HDFs, as some observed globular clusters show different populations separated by sharp differences in helium abundances. The HDFs of the models illustrated in Fig. 4 are shown in Fig. 5. We now briefly discuss this figure:

Panel a - This panel shows that in the RMMPRM the vast majority of the stars have $Y \sim 0.25$, with a thin tail extending up to $Y = 0.37$. For smaller amounts of pristine gas (dashed histogram) the left peak is lowered and shifted toward larger values of Y (for the same reason, the cusp of the dashed line in panel *a* of Fig. 4 is shifted compared to the RMMPRM cusp). The tail in the range $0.29 < Y < 0.33$, as well as the secondary peak at $Y = 0.37$, increase their relative importance.

Panel b - The temporal shift of pristine gas accretion produces its major effects on the secondary, helium rich peak. If the accretion is delayed (RMTACM, dotted line), a larger number of stars form with the pure, He-rich, AGB ejecta, giving rise to a non-negligible secondary peak at $Y = 0.37$. With an early accretion (dashed line) this peak is substantially erased because only few stars form with such a high Y value as the system quickly accretes pristine gas forming the main peak at $Y \sim 0.26$. Later on, as discussed in the previous subsection, most of the pristine gas is depleted by the SF and the ISM is composed of a larger fraction of He-rich AGB ejecta; thus the stars forming at this stage give rise to the HDF secondary peak at $Y \sim 0.32$.

Panel c - From panel *c* of Fig. 4 we have seen that in the model with larger τ (RMATAUM, dotted line) the cusp is slightly brought forward; for the same reason the main peak of the RMATAUM HDF is shifted a little “rightward”. The greater height of the secondary peak at $Y = 0.37$ in the RMATAUL (dashed histogram) is due to the longer time during which the stars form from pure AGB ejecta, before the accretion becomes substantial.

Panel d - The RMEFFL (dashed histogram) creates little less O-poor, He-rich stars at early times, and the HDF shows

therefore a slightly lower secondary peak at $Y = 0.37$. A smaller ν leads to a longer persistence of the pristine gas and of its effect on the ISM chemical characteristics. For this reason the cusp of the dashed curve is shifted “upward” in panel *d* of Fig. 4, and the dashed HDF is shifted “rightward” in the present panel.

Panel e - The models shown in panel *e* differ by the evolutionary time. Although the chemical paths are identical, the HDFs are quite different and reflect the different stellar crowding of the two arms (cf. panel *e* of Fig. 4). The RMTNDL histogram (shorter evolution) shows two well defined populations: a minor one with $Y > 0.35$, and the major one peaked around $Y = 0.26$. In the RMTNDM histogram a third population is present at $Y = 0.31$ as a consequence of the longer permanence of the model on the rising branch.

Panel f - Given the larger amount of AGB ejecta in the RMFGDM (red dotted line), its He-rich peak is higher than in the RMFGDL. The dotted histogram also shows an intermediate population in the range $0.3 < Y < 0.35$ which is substantially absent in the dashed histogram. This intermediate population is a consequence of the bending toward lower values of O of the rising branch of the RMFGDM in the $[\text{O}/\text{Fe}]-[\text{Na}/\text{Fe}]$ plane.

5.2.3 Delayed star formation

As pointed out in 2.1, in some clusters such as ω Cen and NGC 2808 multiple discrete populations are present, each characterized by a specific helium abundance. This led Renzini (2008) to argue that helium-rich material was accumulated in the ISM for a sufficient long time until suddenly a burst turned a major fraction of the ISM into stars. According to this author, a continuous SF proceeding along with the ISM helium enrichment would have resulted in a continuous distribution of helium abundances in the newly formed stars, hence in a broadening of the MS rather than in well separated sequences as actually observed.

In all the models we discussed so far the SF starts “ab initio”, as soon as the ejecta of the massive AGB stars begins to collect within the GC. To investigate the effect of a SF burst we run two models in which the gas cumulates in the GC since the beginning as usual, but with the SF inhibited up to the time $t_{\text{b},7} = 5$ (RMTSFL, blue dashed line) and $t_{\text{b},7} = 7$ (RMTSFM, red dotted line). The chemical patterns are very similar (see the lower panel in Fig. 6), but with the dotted cusp shifted 0.1 dex “leftward” and “upward” compared to the dashed one. In fact, in the RMTSFM a large amount of AGB ejecta gathers before the occurrence of the SF; the dilution by the pristine gas is therefore less effective and the cusp takes place earlier. In this latter model the stars are essentially distributed along the rising branch, as expected given the large SF delay.

In RMTSFM the effects of the pristine gas are less effective, and the primary peak of the HDF (see the upper panel in Fig. 6) is higher and shifted rightward (reflecting the shift of the cusp of dotted line in the lower panel of Fig. 6). The secondary peak is absent because the SF was not active in the beginning, when the gas was very helium-rich. This simple experiment shows that, with a SF delay large enough, it is possible to obtain a sharp intermediate population, but to the expense of the extreme one. Both populations can not be achieved with this mechanism.

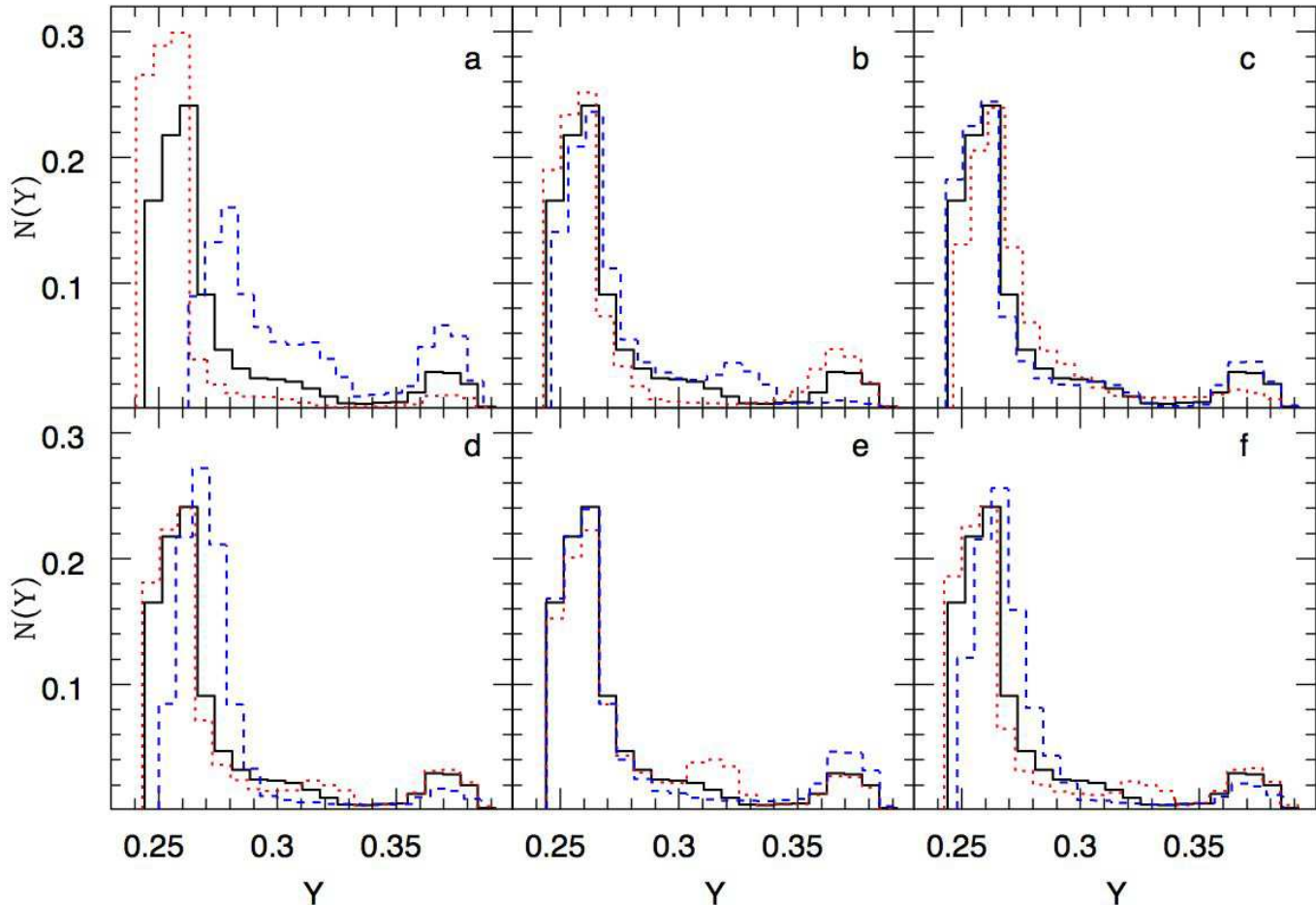


Figure 5. Stellar helium distribution function for different models. The models in each panel are the same shown in the corresponding panel of Fig. 4

6 COMPARISON WITH REAL CLUSTERS

In this section we apply the chemical evolution framework described in the previous section to build two specific models for NGC 2808 and M4. These two clusters are indeed good prototypes to exemplify the cluster to cluster differences. NGC 2808 is a complex mixture of populations, one of which is very extreme, and has a very high helium content testified by the presence of the blue main sequence. M4 is much less massive, and shows milder variations in elemental abundances, particularly in oxygen, but it apparently has a larger spread in sodium. It is to be preferred to other samples also because a very accurate recent spectroscopic survey (Marino et al. 2008b)

6.1 NGC2808

The cluster NGC 2808 has a mass $M \sim 1.6 \times 10^6 M_{\odot}$, and harbours three main populations, as initially speculated by D’Antona & Caloi (2004) and successively confirmed by Piotto et al. (2007). Each population has a distinct helium abundance: $\sim 50\%$ of the stars are credited with a primordial helium abundance ($Y = 0.25$), $\sim 32\%$ with $Y \sim 0.30$ and $\sim 18\%$ with $Y \sim 0.37$ (Carretta et al. 2009c;

D’Antona & Caloi 2008). No iron abundance difference is present in these populations, but they show an extended $[O/Fe]$ - $[Na/Fe]$ anticorrelation (Carretta et al. 2006).

This anticorrelation is apparent in the bottom-left panel of Fig. 7 which includes data obtained with the ESO high-resolution multifiber spectrograph FLAMES/GIRAFFE at VLT by Carretta et al. (2009c) and data obtained with the higher resolution UVES spectrograph (Carretta et al. 2009b).

We simulated the GC NGC 2808 with a model with the parameter set $(t_{ac,7}, t_{end,7}, \tau_7, \rho_{pr}, \rho_{*,FG}, \nu, x) = (5, 6, 0.3, 2.36, 241, 1, 0.5)$. The choice of $x = 0.5$ is done in order to get a current 50% of FG stars, as suggested by the helium abundance; this produces a more realistic comparison with the observations.

The time evolution of the ISM chemical composition is illustrated in Fig. 8; as shown in this figure, owing to the relative shortness of the evolutionary time the C+N+O abundance remains essentially constant in this model. We remind that the absence of a substantial CNO increment is an essential constrain for any model describing the chemistry of the majority of GCs (cf. sect. 2.4).

The cyan circles in the bottom-left panel of Fig. 7 represent a statistical sample of the SG stars obtained integrating

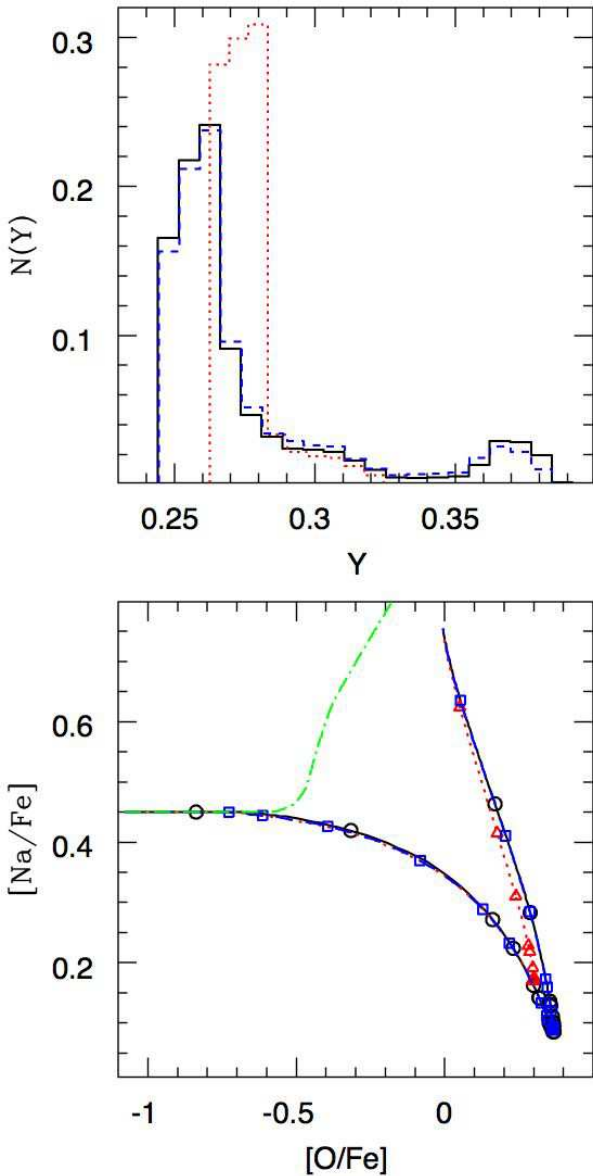


Figure 6. Helium distribution function (upper panel) and chemical pattern (lower panel) of RM (solid line), RMTSFL (blue dashed line) and RMTSFM (red dotted line). The green dot-dashed line indicates the evolution of RMNOPG.

the equation system in sect. 4. In populating the $[\text{O}/\text{Fe}]$ - $[\text{Na}/\text{Fe}]$ plane with such circles, we introduce a stochastic error in the range 0-0.1 dex, comparable to the observational errors, scattering the position of the stars.

The blue circles represent the FG stars. Since the FG stellar population is assumed to be present “ab initio” in our model, these stars are not an outcome of the model, but are included in the figure to ease the comparison with the observational data. The pristine gas from which these stars formed is assumed to have $[\text{O}/\text{Fe}]=0.4$ and $[\text{Na}/\text{Fe}]=0$ and also in this case we introduce a stochastic error in the range 0-0.1 dex in the abundances. The relative number of FG and SG stars is given by the value of the parameter x . Following the terminology of Carretta et al. (2008), the blue circles reproduce the Primordial population, while the cyan ones

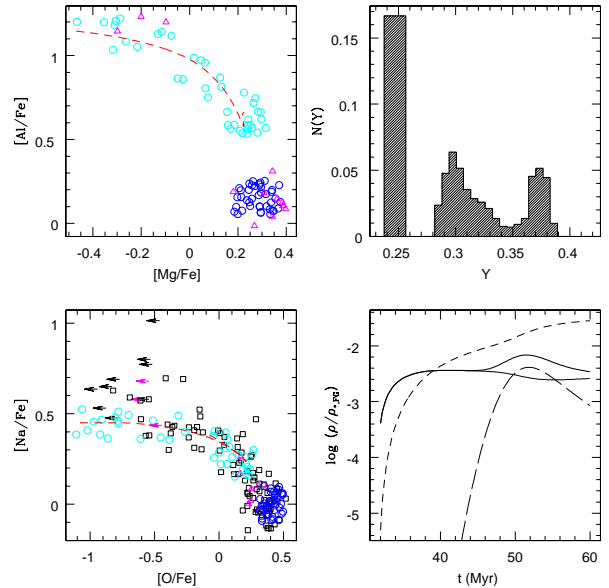


Figure 7. Results of our model for NGC2808. The following set of parameters has been assumed: $(t_{\text{ac},7}, t_{\text{end},7}, \tau_7, \rho_{\text{pr}}, \rho_{*,\text{FG}}, \nu, x) = (5, 6, 0.3, 2.36, 241, 1, 0.5)$. The top-left panel and the bottom-left panel show the $[\text{Mg}/\text{Fe}]$ - $[\text{Al}/\text{Fe}]$ and the $[\text{O}/\text{Fe}]$ - $[\text{Na}/\text{Fe}]$ diagrams relative to NGC 2808, respectively. The black squares and arrows are data obtained with the ESO high-resolution multifiber spectrograph FLAMES/GIRAFFE at VLT by Carretta et al. (2006). Magenta triangles and arrows are data obtained with the higher resolution UVES spectrograph (Carretta et al. 2009b). The blue and cyan circles represent a sampling of the FG and SG stars by our model, respectively. The red dashed line represents the gas trajectory within the diagram; the sampled stars in principle would be located on this line, but we introduced a random scatter in the range 0 - 0.1 dex in their coordinates in order to mimic the observational errors (see text for more details). The top-right panel illustrates the stellar helium distribution function. In the bottom-right panel the evolution of the following quantities is reported: total amount of gas (bold solid line), stellar ejecta (solid line), pristine gas (long-dashed line), SG stars (dashed line).

give the Intermediate and Extreme ($[\text{O}/\text{Fe}] < -0.4$) populations. We emphasize that without the modification in the chemical composition of the FG stars discussed above (cf. sect. 2.2) the Extreme population and part of the Intermediate ones could not be reproduced. In any case, stars with $[\text{Na}/\text{Fe}] > 0.5$ remain unexplained, and suggest that a further parameter is at work. In order to obtain a better fit of the data points, we could have increased the sodium produced in the mass range $6.5 - 9 M_{\odot}$ to $[\text{Na}/\text{Fe}] \sim 0.7$. This procedure has two negative implications: first, it can not explain, in any case, the six points at $[\text{Na}/\text{Fe}] > 0.7$ having upper limits for the oxygen values. In addition, such an extrapolation, implying an increase of the sodium yield with increasing initial mass, is not compatible with our present understanding of the super-AGB evolution (see Sect. 2.1). We prefer then to postpone a better solution of this problem to when more data (e.g., when the oxygen abundance for these stars will be measured) and better models will be available. The imperfect reproduction of these (few) data is not an argument to believe that the origin of the gas forming these SG stars must be looked for somewhere else

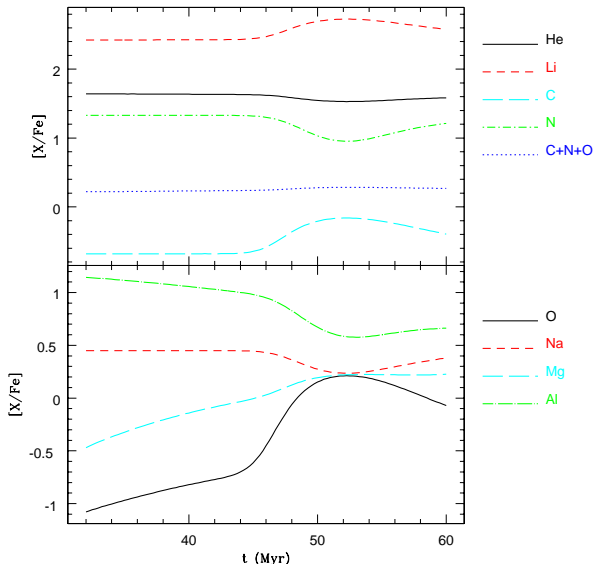


Figure 8. Time evolution of the chemical abundances in the ISM of the NGC 2808 model.

than among super-AGBs. In fact, no other source can be able to deal, at the same time, with the reproduction of the Mg-poor, Al-rich stars (Decressin et al. 2007), and with the extreme but homogeneous helium content that is necessary to reproduce the triple main sequence (D’Ercole et al. 2008; D’Antona & Caloi 2008; Renzini 2008, and Fig. 7, top right panel). In summary, we regard the fit of NGC 2808 data as very satisfactory, in spite of this remaining problem.

The three [Al/Fe]-rich stars in the upper-left panel of Fig. 7 coincide with the three magenta arrows in the [O/Fe]-[Na/Fe] diagram. In both diagrams these UVES data (Carretta et al. 2009b) show a very “clumpy” anticorrelation, with only Primordial and Extreme populations present, and a gap in the middle where no star is found. On the other hand, our model, giving rise to stars occurring throughout the whole O-Fe anticorrelation span, necessarily produces a “continuous” distribution of stars in the [Mg/Fe]-[Al/Fe] diagram. We believe that the gap in the Mg-Al anticorrelation displayed by the UVES data is not real (as indeed shown by the FLAMES/GIRAFFE data (Carretta et al. 2009c) in the [O/Fe]-[Na/Fe] plane), and we predict that an Intermediate population in the [Mg/Fe]-[Al/Fe] diagram will be observed in the next future.

Finally, the top-right panel of Fig. 7 shows the helium stellar distribution. Three stellar populations are clearly present. The most He-rich stellar group ($Y > 0.35$) originates from the FG ejecta before the pristine gas enters the GC, while the Intermediate population ($0.3 \lesssim Y < 0.35$) forms after the accretion of the original gas. The ratio between Extreme and Intermediate He-rich stars is 0.56, as observed. Contrary to the abundance of the FG stars, which is simply imposed, the value of the ratio between Extreme and Intermediate stars is a genuine result of our model.

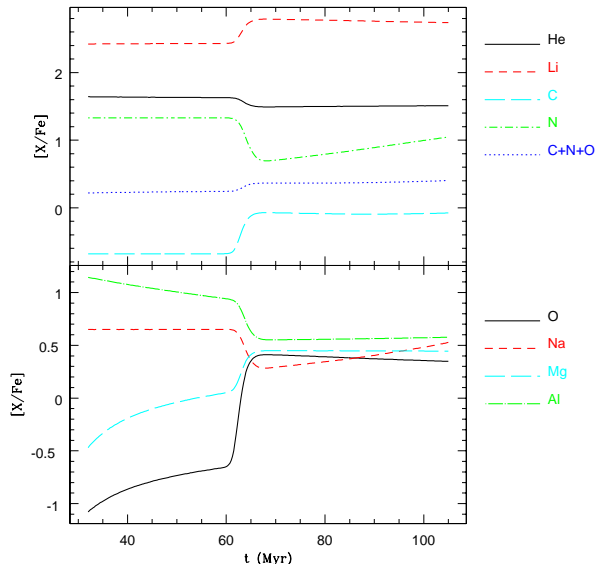


Figure 9. Time evolution of the chemical abundances in the ISM of the M4 model.

6.2 M4 (NGC 6121)

The globular cluster M4 has a mass $M = 6.3 \times 10^4 M_{\odot}$ (Mandushev et al. 1991) and its color-magnitude diagram does not show any of the fingerprints of the presence of multiple populations found in the most massive clusters. However, the O-Na anticorrelation is present in this cluster as in all the Galactic GCs. Instead, contrary to NGC 2808, there is no Mg-Al anticorrelation in M4 (Marino et al. 2008b). As the stellar evolution must be the same in all the GCs, our aim is to fit M4 data adopting the same chemical composition of the AGB ejecta utilized in modelling NGC 2808. However, we must assume a different composition of the pristine gas. This can be understood by looking at the observational data in Fig. 7 and 10. The FG oxygen, sodium, magnesium and aluminium for NGC 2808 are $[O/Fe] \sim +0.4$, $[Na/Fe] \sim 0.0$, $[Mg/Fe] \sim +0.28$ and $[Al/Fe] \sim +0.15$. In M4 we have $[O/Fe] \sim +0.5$, $[Na/Fe] \sim +0.1$, $[Mg/Fe] \sim +0.5$ and $[Al/Fe] \sim +0.4$. Therefore, with respect to the input values for NGC 2808, in the present model we adopt O and Na abundances 25% higher, and Mg and Al abundances 67% and 78% higher, respectively. As a consequence, we should also consider that the *initial* abundance of ^{20}Ne , another α element, may have been larger in the pristine gas. Following the test computations described in section 2.2, also the sodium yield of the AGBs will be larger, and we can reasonably increase by a factor 0.2 dex the ratio $[Na/Fe]$ of the ejecta of the AGB of any mass. Notice that this last change in the yield table is only applied to the M4 case, due to the different initial chemistry of its FG.

For this model of M4 we set the parameters $(t_{ac,7}, t_{end,7}, T_7, \rho_{pr}, \rho_{*,FG}, \nu, x) = (6.5, 10.5, 0.91, 9.4, 0.1, 0.7)$. The results are illustrated in Fig. 9 and Fig. 10. The former figure shows the evolution of the ISM chemical abundance of several elements; in particular, it can be seen that the variation of C+N+O abundance is not larger than 0.1 dex, as required by the

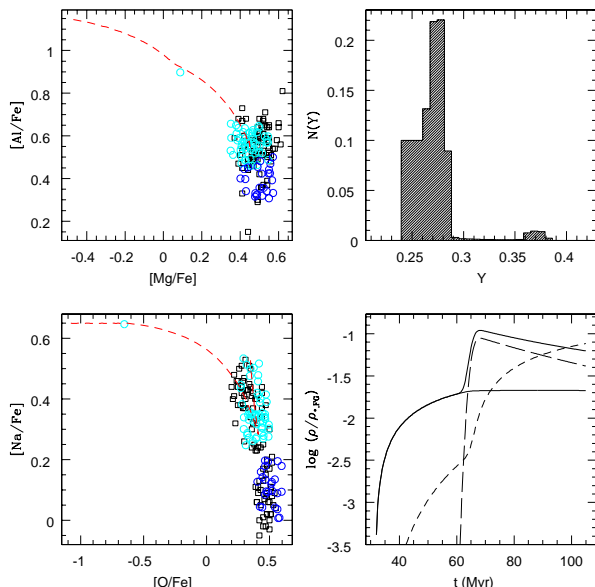


Figure 10. As Fig. 7, but for M4. Data are from Marino et al. (2008b). In this case, for a better comparison with the data, the error on $[\text{Na}/\text{Fe}]$ is taken 0.05 dex instead of 0.1 dex as in the case of NGC 2808.

observations (Yong et al. 2009). Figure 10 can be compared to the analogous Fig. 7 relative to NGC 2808 to understand the different role played by various parameters in the two cases.

Our model shows that the relative amount of pristine gas must be larger than in NGC 2808. The reason is illustrated in the bottom-left panel of Fig. 10. The Na-O anticorrelation is less extended than in NGC 2808; in particular, all the stars in M4 exhibit a positive ratio $[\text{O}/\text{Fe}]$, while in NGC 2808 stars are found with ratios as low as $[\text{O}/\text{Fe}] \sim -1$. In order to reduce the fraction of this kind of stars we set $\nu = 0.1$ so to minimize the SFR in the beginning, before the accretion of pristine gas, when the ISM is composed only of O-poor AGB ejecta. After the pristine gas accretion and the consequent increase of the ISM density, the SFR becomes significant despite the low value of ν . Thus, a large fraction of SG stars form from an ISM strongly “diluted” by the pristine O-rich gas.

In order to form the observed Na-rich stars, the model for M4 also requires a value of t_{end} larger than that of NGC 2808. By extending the SF duration, Na-rich stars can form at late time when the pristine gas has been strongly depleted by SF and the ISM is mainly composed of the Na-rich stellar ejecta of stars with $M < 6 M_{\odot}$.

The chemical evolution of the GC is summarized by the dashed line in the bottom-left panel of Fig. 10. The model starts at the O-poor extreme and moves rightward relatively fast and in a low SFR regime, so that only $\sim 3\%$ of the total SG population form during this excursion. The trajectory has a cusp at $[\text{O}/\text{Fe}] \sim 0.4$ where then develops a rather vertical branch due to the reduction of pristine gas and the increment of Na-rich ejecta in the ISM “mixture”. The longer length of time spent along this branch and, more importantly, the larger SFR during this stage determine the

clustering of the SG stellar population in this area of the Na-O plane.

The amount of pristine gas accreted by the GC is a key parameter to fit the observed data *both* in the $[\text{O}/\text{Fe}]-[\text{Na}/\text{Fe}]$ and the $[\text{Mg}/\text{Fe}]-[\text{Al}/\text{Fe}]$ diagrams. An increment of pristine gas causes the abundances of SG stars to approach those of FG stars and, in particular, reduces the differences in the $[\text{Na}/\text{Fe}]$ and $[\text{Al}/\text{Fe}]$ ratios between Primordial and Intermediate stars. The Na abundance is, however, more sensitive to this effect: a model of ours (not shown here) reveals that, after trebling the accreted gas, the Al abundances are still consistent with the data, while stars with $[\text{Na}/\text{Fe}] > 0.4$ can not be reproduced.

Finally, from the top-right panel of Fig. 10 we note that the helium abundance of the SG Intermediate population is not much larger than that of the FG one, and the two populations, although still distinguishable, blend together in the HDF. This small helium spread can be revealed in careful observations of the main sequence width (see, e.g., the analysis by Milone et al. 2010, for the cluster NGC 6752) and for its possible consequences on the horizontal branch (HB) morphologies (D’Antona & Caloi 2008). The HB of M4 shows signs of bimodality (Norris 1981) but a careful representation of the data is very tricky, as it requires use of models including also the CNO abundance enhancements of the SG (see the discussion by Salaris et al. 2008, concerning the bimodal distribution in the HB of NGC 1851). D’Antona et al. (2009) notice that the blue side of the HB of M4 might be slightly overluminous with respect to the blue HB of NGC 1851, and tentatively attribute this feature to possible helium enhancement in these stars. This would be consistent with our helium distribution in M4.

The Extreme population is still present, but is only 2% of the whole GC stellar population. As observationally this population is lacking in the clusters that are not very massive, this may be an indication that the formation of the Extreme population is inhibited below some critical mass. Alternatively, given its paucity, we can guess that this population exists but is not yet observed⁶.

In any case, as shown in sect. 5.2, it is enough to change somewhat one or more parameters to create or remove small structures in the helium distribution function. Thus, at this stage, no firm conclusion can be drawn on the Extreme population we found, or on the detailed helium spread of the Intermediate population. More realistic models are planned, in which the chemical machinery developed in this paper will be implemented in a hydro-code.

7 CONCLUSIONS

In this paper we have studied the origin of the chemical patterns which have been observed in many globular clusters and which are considered the spectroscopic fingerprints of the presence of multiple stellar populations. Specifically, in our investigation we have focussed our attention on the O-Na and Mg-Al anticorrelations and the helium distribution function.

⁶ Notice however that a very helium rich, even small, population would be photometrically very evident, as it would populate the extreme blue horizontal branch (D’Antona & Caloi 2008).

In our model we have assumed that AGB stars are the polluting source of gas with the anomalous abundances of light elements observed in globular cluster second-generation stars. Our chemical framework is based on a one-zone model following the formation of SG stars from a mix of ejecta of AGB stars and pristine gas.

We have carried out a large number of simulations to explore the dependence of the SG chemical properties on the parameters characterizing the star formation process and the dynamics of the involved pristine gas. Finally, we have used our framework to model the observed chemical patterns in the Galactic clusters NGC 2808 and M4.

The main results of our study are the following:

(i) The current stellar models provide AGB ejecta in which both Na and O decrease with increasing stellar mass. In order to reproduce the observed O-Na anticorrelation, the gas from which SG stars form must be diluted with O-rich, Na-poor pristine gas (see e.g. Figs. 2 and 3).

(ii) The amount of pristine gas involved in the SG formation process, the timescales driving the dynamics of such gas, and the star formation efficiency play a key role in determining the extension of the O-Na anticorrelation and the fraction of extreme Na-rich/O-poor stars.

(iii) The helium abundance distribution function is correlated with the distribution of stars in the O-Na plane. Extreme Na-rich/O-poor stars are also those with an extreme He enrichment. Our models predict that all the clusters with a very extended O-Na anticorrelation should also host a population of He-rich stars.

(iv) Our models show that the extension of the O-Na anticorrelation is closely correlated with that in the Mg-Al plane; Na-rich/O-poor stars have also high Al and low Mg abundances.

(v) We have used our framework to build specific models for two prototypical Galactic globular clusters: NGC 2808, a massive cluster that hosts a SG population characterized by a very extended O-Na anticorrelation and includes a very He-rich population, and M4, a low-mass cluster with a significantly less extended O-Na anticorrelation that does not include extremely Na-rich O-poor stars and for which there is no photometric evidence of a He-rich population. Despite the significant differences in their chemical patterns, in both clusters a significant fraction of stars belong to the SG (50 per cent in NGC 2808, Carretta et al. 2009c, and 65 per cent in M4 Carretta et al. (2009c); Marino et al. (2008b)).

Our models successfully reproduce the differences in the O-Na anticorrelation observed in these two clusters, the distribution of stars in the Mg-Al plane in M4 and predict an extended Mg-Al anticorrelation for NGC 2808. Al and Mg abundances for NGC 2808 have been determined with UVES observations only for a small number of either Na-rich/O-poor or Na-poor/O-rich stars. As predicted by our model, these stars populate only the Al-rich/Mg-poor and the Al-poor/Mg-rich regions of the Mg-Al plane. According to our model, future determinations of Al and Mg abundances of targeting stars with intermediate Na and O should lead to intermediate Al and Mg abundances filling the extended Al-Mg anticorrelation.

(vi) The helium distribution, including the extreme population formed directly from super-AGB ejecta is well reproduced by our model for NGC 2808 (see Fig. 7). In clusters

like M4, in which a larger dilution with pristine matter is necessary to model the O-Na and Mg-Al patterns, a large helium dispersion is not required, but a small helium spread should generally be present (see Fig. 10).

Our investigation has shed light on the key chemical and hydrodynamical ingredients determining the formation of the chemical patterns observed in globular clusters. The results presented here are to be the starting point informing further study based on full hydrodynamical simulations. Several issues will require further investigation. Specifically, as for the stellar evolution models, we have shown that our conservative choice of an educated linear and monotonic extrapolation for the sodium and oxygen abundances in the mass range from 6.5 to 9 M_{\odot} reproduces the general trend of the O-Na anticorrelations of different clusters, when also the differences in neon abundances in the FG of different clusters are taken into account. In NGC 2808, however, we can not reproduce the (few) very large sodium values of some stars for which only upper limits on the oxygen abundance are available (see Fig. 7). Another parameter is probably at work here, and only further investigation into the super-AGB phase will shed light on this issue.

The lack of any evidence of a significant metal enrichment in most clusters hosting multiple stellar populations implies that neither ejecta from FG nor SG supernovae is involved in the chemical enrichment of matter from which SG stars form. While in our model SG formation starts after the end of the FG SN II epoch, it is to be further clarified whether the lack of metal enrichment from SG supernovae is due to SG forming with IMF truncated at $M < 9 M_{\odot}$ or whether this is a consequence of a more complex gas dynamics to be further explored with full hydrodynamical simulations.

Finally, additional full hydrodynamical simulations will be needed to clarify the source of pristine gas and the accretion mechanism. Different processes have been considered in the literature, such as accretion from a diffuse surrounding medium (e.g. Lin & Murray 2007; Pflamm-Altenburg & Kroupa 2009) or interaction with molecular clouds (Bekki & Mackey 2009). Conditions for an effective gas collection within the cluster turn out to be rather specific. Instead, our model requires a mechanism general enough to work in all the clusters and able to take into account the cluster-to-cluster differences in the dynamics and the amount of pristine gas involved in the SG formation process.

ACKNOWLEDGMENTS

We are grateful to E. Carretta and A. Renzini for useful discussions. A.D. acknowledges financial support from Italian MIUR through grant PRIN 2007, prot. 2007JJC53X. F.D. and P.V. have been supported through PRIN MIUR 2007 “Multiple stellar populations in globular clusters: census, characterization and origin” (prot. n. 20075TP5K9). E.V. and S.M. were supported in part by NASA grant NNX10AD86G.

REFERENCES

- Angulo C., Arnould M., Rayet M., Descouvemont P., Baye D., Leclercq-Willain C., Coc A., Barhoumi S., Aguer P., Rolfs C., Kunz R., Hammer J. W., Mayer A., Paradellis T., Kossionides S., Chronidou C., Spyrou K., degl’Innocenti S., Fiorentini G., Ricci B., Zavatarelli S., Providencia C., Wolters H., Soares J., Grama C., Rahighi J., Shotter A., Laméhi Rachti M., 1999, *Nuclear Physics A*, 656, 3
- Asplund M., Grevesse N., Sauval A. J., Scott P., 2009, *ARA&A*, 47, 481
- Bedin L. R., Piotto G., Anderson J., Cassisi S., King I. R., Momany Y., Carraro G., 2004, *ApJ*, 605, L125
- Bekki K., Campbell S. W., Lattanzio J. C., Norris J. E., 2007, *MNRAS*, 377, 335
- Bekki K., Mackey A. D., 2009, *MNRAS*, 394, 124
- Bellazzini M., Ibata R. A., Chapman S. C., Mackey A. D., Monaco L., Irwin M. J., Martin N. F., Lewis G. F., Dalessandro E., 2008, *AJ*, 136, 1147
- Busso G., Cassisi S., Piotto G., Castellani M., Romaniello M., Catelan M., Djorgovski S. G., Recio Blanco A., Renzini A., Rich M. R., Sweigart A. V., Zoccali M., 2007, *A&A*, 474, 105
- Caloi V., D’Antona F., 2007, *A&A*, 463, 949
- Carretta E., Bragaglia A., Gratton R., D’Orazi V., Lucatello S., 2009a, *A&A*, 508, 695
- Carretta E., Bragaglia A., Gratton R., Lucatello S., 2009b, *A&A*, 505, 139
- Carretta E., Bragaglia A., Gratton R., Lucatello S., Bellazzini M., D’Orazi V., 2010, *ArXiv e-prints*
- Carretta E., Bragaglia A., Gratton R. G., Leone F., Recio-Blanco A., Lucatello S., 2006, *A&A*, 450, 523
- Carretta E., Bragaglia A., Gratton R. G., Lucatello S., 2008, *ArXiv e-prints*
- Carretta E., Bragaglia A., Gratton R. G., Lucatello S., Catanzaro G., Leone F., Bellazzini M., Claudi R., D’Orazi V., Momany Y., Ortolani S., Pancino E., Piotto G., Recio-Blanco A., Sabbi E., 2009c, *A&A*, 505, 117
- Carretta E., Gratton R. G., Lucatello S., Bragaglia A., Bonifacio P., 2005, *A&A*, 433, 597
- Cassisi S., Salaris M., Pietrinferni A., Piotto G., Milone A. P., Bedin L. R., Anderson J., 2008, *ApJ*, 672, L115
- Choi E., Yi S. K., 2008, *MNRAS*, 386, 1332
- Ciotti L., Pellegrini S., Renzini A., D’Ercole A., 1991, *ApJ*, 376, 380
- Cohen J. G., Meléndez J., 2005, *AJ*, 129, 303
- Da Costa G. S., Held E. V., Saviane I., Gullieuszik M., 2009, *ApJ*, 705, 1481
- D’Antona F., Bellazzini M., Caloi V., Pecci F. F., Galletti S., Rood R. T., 2005, *ApJ*, 631, 868
- D’Antona F., Caloi V., 2004, *ApJ*, 611, 871
- , 2008, *MNRAS*, 390, 693
- D’Antona F., Stetson P. B., Ventura P., Milone A. P., Piotto G., Caloi V., 2009, *MNRAS*, 399, L151
- D’Antona F., Ventura P., 2007, *MNRAS*, 379, 1431
- Decressin T., Meynet G., Charbonnel C., Prantzos N., Ekström S., 2007, *A&A*, 464, 1029
- Denissenkov P. A., Herwig F., 2003, *ApJ*, 590, L99
- D’Ercole A., Vesperini E., D’Antona F., McMillan S. L. W., Recchi S., 2008, *MNRAS*, 391, 825
- Ferraro F. R., Dalessandro E., Mucciarelli A., Beccari G., Rich R. M., Origlia L., Lanzoni B., Rood R. T., Valenti E., Bellazzini M., Ransom S. M., Cocozza G., 2009, *Nature*, 462, 483
- Gratton R., Sneden C., Carretta E., 2004, *ARA&A*, 42, 385
- Gratton R. G., Bonifacio P., Bragaglia A., Carretta E., Castellani V., Centurion M., Chieffi A., Claudi R., Clementini G., D’Antona F., Desidera S., François P., Grundahl F., Lucatello S., Molaro P., Pasquini L., Sneden C., Spite F., Straniero O., 2001, *A&A*, 369, 87
- Hale S. E., Champagne A. E., Iliadis C., Hansper V. Y., Powell D. C., Blackmon J. C., 2002, *Phys. REV. C*, 65, 015801
- Herwig F., 2004, *ApJS*, 155, 651
- Ivans I. I., Kraft R. P., Sneden C., Smith G. H., Rich R. M., Shetrone M., 2001, *AJ*, 122, 1438
- Ivans I. I., Sneden C., Kraft R. P., Suntzeff N. B., Smith V. V., Langer G. E., Fulbright J. P., 1999, *AJ*, 118, 1273
- Izzard R. G., Lugaro M., Karakas A. I., Iliadis C., van Raai M., 2007, *A&A*, 466, 641
- Johnson C. I., Pilachowski C. A., Michael Rich R., Fulbright J. P., 2009, *ApJ*, 698, 2048
- Karakas A., Lattanzio J. C., 2007, *Publications of the Astronomical Society of Australia*, 24, 103
- Karakas A. I., Fenner Y., Sills A., Campbell S. W., Lattanzio J. C., 2006, *ApJ*, 652, 1240
- Kraft R. P., Ivans I. I., 2003, *PASP*, 115, 143
- Lee J., Lee J., Kang Y., Lee Y., Han S., Joo S., Rey S., Yong D., 2009, *ApJ*, 695, L78
- Lin D. N. C., Murray S. D., 2007, *ApJ*, 661, 779
- Mandushev G., Staneva A., Spasova N., 1991, *A&A*, 252, 94
- Marcolini A., Sollima A., D’Ercole A., Gibson B. K., Ferraro F. R., 2007, *MNRAS*, 382, 443
- Marino A. F., Milone A. P., Piotto G., Villanova S., Bedin L. R., Bellini A., Renzini A., 2009, *A&A*, 505, 1099
- Marino A. F., Villanova S., Piotto G., Milone A. P., Momany Y., Bedin L. R., Medling A. M., 2008a, *A&A*, 490, 625
- , 2008b, *A&A*, 490, 625
- Matteucci F., Greggio L., 1986, *A&A*, 154, 279
- Milone A. P., Bedin L. R., Piotto G., Anderson J., King I. R., Sarajedini A., Dotter A., Chaboyer B., Marín-Franch A., Majewski S., Aparicio A., Hempel M., Paust N. E. Q., Reid I. N., Rosenberg A., Siegel M., 2008, *ApJ*, 673, 241
- Milone A. P., Piotto G., King I. R., Bedin L. R., Anderson J., Marino A. F., Momany Y., Malavolta L., Villanova S., 2010, *ApJ*, 709, 1183
- Norris J., 1981, *ApJ*, 248, 177
- Norris J., Freeman K. C., Da Costa G. S., 1984, *ApJ*, 277, 615
- Norris J. E., 2004, *ApJ*, 612, L25
- Pflamm-Altenburg J., Kroupa P., 2009, *MNRAS*, 397, 488
- Piotto G., Bedin L. R., Anderson J., King I. R., Cassisi S., Milone A. P., Villanova S., Pietrinferni A., Renzini A., 2007, *ApJ*, 661, L53
- Piotto G., Villanova S., Bedin L. R., Gratton R., Cassisi S., Momany Y., Recio-Blanco A., Lucatello S., Anderson J., King I. R., Pietrinferni A., Carraro G., 2005, *ApJ*, 621, 777
- Prantzos N., Charbonnel C., Iliadis C., 2007, *A&A*, 470,

179

- Pumo M. L., D'Antona F., Ventura P., 2008, *ApJ*, 672, L25
Ramírez S. V., Cohen J. G., 2002, *AJ*, 123, 3277
Renzini A., 2008, *MNRAS*, 391, 354
Rich R. M., Sosin C., Djorgovski S. G., Piotto G., King I. R., Renzini A., Phinney E. S., Dorman B., Liebert J., Meylan G., 1997, *ApJ*, 484, L25+
Romano D., Matteucci F., Tosi M., Pancino E., Bellazzini M., Ferraro F. R., Limongi M., Sollima A., 2007, *MNRAS*, 376, 405
Salaris M., Cassisi S., Pietrinferni A., 2008, *ApJ*, 678, L25
Sarajedini A., Layden A. C., 1995, *AJ*, 109, 1086
Siess L., 2007a, *A&A*, 476, 893
—, 2007b, in *Astronomical Society of the Pacific Conference Series*, Vol. 378, *Why Galaxies Care About AGB Stars: Their Importance as Actors and Probes*, Kerschbaum F., Charbonnel C., Wing R. F., eds., pp. 9+
Snedden C., Kraft R. P., Guhathakurta P., Peterson R. C., Fulbright J. P., 2004, *AJ*, 127, 2162
Suntzeff N., 1993, in *Astronomical Society of the Pacific Conference Series*, Vol. 48, *The Globular Cluster-Galaxy Connection*, G. H. Smith & J. P. Brodie, ed., pp. 167+
Ventura P., Caloi V., D'Antona F., Ferguson J., Milone A., Piotto G. P., 2009, *MNRAS*, 399, 934
Ventura P., D'Antona F., 2005a, *A&A*, 431, 279
—, 2005b, *A&A*, 439, 1075
—, 2006, *A&A*, 457, 995
—, 2008a, *MNRAS*, 385, 2034
—, 2008b, *A&A*, 479, 805
—, 2009, *A&A*, 499, 835
Wheeler J. C., Snedden C., Truran Jr. J. W., 1989, *ARA&A*, 27, 279
Yong D., Grundahl F., D'Antona F., Karakas A. I., Lattanzio J. C., Norris J. E., 2009, *ApJ*, 695, L62
Yong D., Grundahl F., Nissen P. E., Jensen H. R., Lambert D. L., 2005, *A&A*, 438, 875
Yoon S.-J., Joo S.-J., Ree C. H., Han S.-I., Kim D.-G., Lee Y.-W., 2008, *ApJ*, 677, 1080